NF

WYLE LABORATORIES - RESEARCH STAFF
REPORT WR 66 - 32

PRELIMINARY ANALYSIS OF THE EFFECTS OF PRESSURE SPACE CORRELATIONS ON THE VIBRATIONS OF APOLLO FLIGHT STRUCTURE

WYLE LABORATORIES
TESTING DIVISION, HUNTSVILLE FACILITY

research

Rot 46679

WYLE LABORATORIES - RESEARCH STAFF
REPORT WR 66 - 32

PRELIMINARY ANALYSIS OF THE EFFECTS OF PRESSURE SPACE CORRELATIONS ON THE VIBRATIONS OF APOLLO FLIGHT STRUCTURE

by

R.W. White
M.J. Crocker

Work Performed Under Contract NAS9-4305
Acoustic Study

Prepared by R.W. White
R.W. White

Approved by Kenneth McK. Eldred
Kenneth McK. Eldred

Prepared by M.J. Crocker
M.J. Crocker

May 1966

COPY NO. 23

SUMMARY

This report contains a preliminary analytical investigation of the vibration response of Apollo skin structure to convected boundary layer turbulence, with emphasis on the variations of the response amplitudes with longitudinal and lateral correlation lengths.

The portion of the Apollo considered is the truncated conical Spacecraft Lunar Excursion Module Adaptor (SLA); and for purposes of this analysis, this structure is treated as an equivalent simply supported, uniform, flat, rectangular, honeycomb plate having essentially the same dynamic characteristics as the SLA. The response spectral density is computed for a pressure space correlation pattern having the functional form of an exponentially damped cosine along, and normal to, the flow axis. By including over 300 modes of the plate, a cursory parameter study is made to show how the response levels of the essentially discrete modes vary with longitudinal and lateral correlation lengths and convection velocities.

TABLE OF CONTENTS

LIST OF FIGURES

LIST OF FIGURES (continued)

LIST OF TABLES

LIST OF SYMBOLS

a	=	length of plate along the x - axis, in.
A	=	longitudinal pressure correlation decay parameter; eq.(35)
b	=	width of plate along the y - axis, in.
C_m	=	bending wave velocity component for m-elastic half waves along the x-axis, in/sec; eq. (27)
$\bar{D}$	=	mean diameter of SLA = 17.8 ft.
E	=	Young's modulus of elasticity, lb./in.^{2}
f	=	excitation and response frequency, cps
f_m	=	resonance frequency of the m-th longitudinal mode of plate, cps; eq. (29)
f_{mn}	=	resonance frequency of mn-mode of plate, cps; eq. (3)
$\mathcal{F}_{mn}(t, \omega)$	=	generalized force for the mn-mode for harmonic excitation at frequency ω, lb; eq. (8)
g	=	acceleration of gravity = 386.4 in./sec.^{2}
h	=	overall thickness of honeycomb plate = 1.70 in.
$\bar{h}$	=	location of neutral bending axis along z-axis of plate = 0.551 in.
$H(\omega/\omega_{mn})$	=	dynamic magnification factor for the mn-mode; eq. (13)
I	=	moment of iniertia of cross-section area per unit of length of the plate = 0.0287 in.^{3}
$J^2_{mn}(\omega)$	=	joint-acceptance of mn-mode at frequency ω; eq. (26)
k_i	=	pressure correlation parameters, i = 1, 2, 3, 4; eq. (43)
$\mathcal{K}_{mn}$	=	generalized stiffness of the mn-mode, lb./in.
m	=	number of elastic half-waves of plate along x-axis
M	=	Mach number
M_o	=	total weight of plate, lb.
$\mathcal{M}_{mn}$	=	generalized weight for the mn-mode, lb; eq. (11)
n	=	number of elastic half-waves of plate along y -axis

P_x, P_y	=	joint-acceptance parameters; eq. (26)
$P(x,y,t;\omega)$	=	instantaneous harmonic pressure acting on plate at point (x,y) at time t and frequency ω, lb./in.^{2}
q_x, q_y	=	joint-acceptance parameters; eq. (26)
Q	=	dynamic magnification factor at resonance
r_x, r_y	=	joint-acceptance parameters; eq. (26)
$R_p(x,y,x',y',\omega)$	=	pressure space cross-correlation function for points (x,y) and (x',y') at frequency ω; eq. (24)
$S_p(\omega)$	=	power spectral density of pressure at frequency ω, $(\text{psi})^2/\text{cps}$
$S_w(x,y;\omega)$	=	power spectral density of plate deflection at point (x,y) and frequency ω, in.^{2}/cps; eq. (21)
$S_{\ddot{w}}(x,y;\omega)$	=	power spectral density of plate acceleration at point (x,y) and frequency ω, $(\text{in./sec.}^2)^2/\text{cps}$; eq. (22)
t	=	time, sec.
U	=	free stream velocity of air flow
U_c	=	turbulent boundary layer convection velocity = 14,400 in./sec.
$W_{mn}(x,y,t;\omega)$	=	instantaneous deflection of the mn-mode at time t and frequency ω, in; eq. (8)
x	=	plate coordinate axis parallel to convected turbulent flow direction
$\bar{x}$	=	nondimensional coordinate = x/a
y	=	plate coordinate axis normal to convected turbulent flow direction
$\bar{y}$	=	nondimensional coordinate = y/b
z	=	plate coordinate normal to surface of plate
γ_x	=	longitudinal pressure correlation length parameter; eq. (25)
γ_y	=	lateral pressure correlation length parameter; eq. (25)
δ_x	=	longitudinal pressure space correlation decay rate; eq. (25)
δ_y	=	lateral pressure space correlation decay rate; eq. (25)
Δ_x, Δ_y	=	joint-acceptance parameters; eq. (26)

ζ	=	separation distance along y-axis = $y - y'$, in.
$\bar{\zeta}$	=	nondimensional form of ζ, = ζ/b
ξ	=	separation distance along x -axis = $x - x'$, in.
$\bar{\xi}$	=	nondimensional form of ξ, = ξ/a
ξ_o	=	first longitudinal zero crossing of pressure correlation pattern, in; eq. (33)
ξ_c	=	longitudinal pressure correlation length, in; eq. (34)
ξ_{mn}	=	generalized mass fraction for the mn-mode.
$\theta(\omega/\omega_{mn})$	=	phase angle between the pressure excitation and the response for the mn-mode at frequency ω.
λ_m	=	bending wave length along x -axis for m elastic half waves along the x-axis; eq. (28)
$\phi_{mn}(x,y)$	=	mode shape of mn-mode of plate; eq. (2)
μ	=	weight per unit area of plate = 2 lb ./ft.^{2}
Φ_x	=	factor for longitudinal component of joint-acceptance; eq. (26)
Φ_y	=	factor for lateral component of joint-acceptance; eq. (26)
ω	=	excitation and response frequency, rad./sec.
ω_{mn}	=	resonance frequency of the mn-mode, rad./sec.
$\Delta\omega$	=	frequency bandwidth, rad./sec.
$\lvert\ \rvert$	=	denotes absolute value
$\overline{(\ )}$	=	denotes time average value

1.0 INTRODUCTION

During its ascent through the atmosphere, the Saturn V launch vehicle with the Apollo Spacecraft will be subjected to severe fluctuating surface pressures which act as the major source of excitation for structural vibrations of the vehicle. These pressures are caused by acoustic noise from the engine exhaust, and unsteady aerodynamic flow over the vehicle, which flows are associated with such mechanisms as wakes, turbulent boundary layers, oscillating shocks and flow separation. Temporally, engine exhaust noise is the predominant source of these pressures in the first ten or twenty seconds of flight, while the unsteady aerodynamic flow dominates the pressure field during the remainder of the atmospheric flight phase, reaching a maximum environment near maximum dynamic pressure. Spatially, the maximum environment caused by engine noise occurs at the aft end of the vehicle in the vicinity of the engines, while the maximum aerodynamic environment occurs at the forward end of the vehicle. Predicted overall pressure levels for the vehicle are shown in Figure 1 for both the fore and aft ends; and it is seen that at the nose, the maximum aerodynamic environment is greater than the acoustic environment. Thus, with respect to the Apollo, the aerodynamic excitation at maximum dynamic pressure is the more severe environment.

During launch, the Apollo is equipped with a rocket escape tower which is situated forward of the Command Module. Because of its poor aerodynamic geometry, the air flow over this tower bathes the vehicle in a turbulent wake which, in addition to causing flow separation, ensures that the boundary layer over the vehicle is everywhere turbulent. Shock waves also form at the flares and shoulders of the vehicle, and during the transonic flight phase, these shock waves tend to oscillate and to progress slowly downward over the vehicle surface causing a severe unsteady pressure loading on the external skin. Although these aerodynamic phenomena are sometimes mutually coupled and sometimes coupled with the ensuing panel vibrations, first order estimates of their effects on structural response can be obtained by neglecting such coupling.

The oscillating shocks are found to be pseudo-discrete in the sense that the frequency spectrum of the surface pressure oscillations shows an energy concentration in a narrow frequency range while the amplitude excursion is random in time. Experimental evidence shows that such shocks are quick to couple with any forcing frequency present in the environment, including panel resonances. The response of panels to sinusoidally oscillating shocks is analyzed in Reference 2 and is not considered in this report.

This report is concerned primarily with the estimation of response levels of Apollo-like structures to turbulent boundary layer pressure fluctuations; and the pressure spectra and spatial correlation properties used in the analysis are typical of those which may occur for in-flight Apollo environments at maximum dynamic pressure. A limited study is also made to show how the response levels vary with longitudinal and lateral

correlation lengths and spatial correlation decay rates, so that the results can be extended to a degree in order to include structural response to separated flow pressure fluctuations. In particular, the turbulent boundary layer parameters are chosen on the basis of the predicted properties of the turbulent flow over the SLA. This section of the Apollo was chosen because the skin structure for this section is the most uniform and the most amenable to analysis - or, the most appropriate for the assumptions which must be made in the analysis.

In Reference 3, Wilby presents an analysis of the response of a simply supported, flat, rectangular plate to convected boundary layer turbulence; and since the complex equation for the joint-acceptance (the normalized mean square of the effective modal forcing function) has been worked out for such a structure and loading, it is desirable to idealize the SLA skin structure to a simply supported, flat, rectangular plate having essentially the same dynamic characteristics as the SLA. The details associated with this simplification are found in Section 2.0 of this report, where the resonance frequencies for several hundred modes are tabulated.

A discussion of the turbulent boundary layer properties and appropriate parameters used in the analysis is presented in Section 3.0 of this report. A summary of turbulence pressure spectra has been developed by Lowson in Reference 4; and, based on laboratory experimental data, Maestrello in Reference 5 has developed an empirical expression for the space correlation function for homogeneous boundary layer turbulence. These two important quantities are discussed in Section 3.0

The general analytical procedure for predicting vibration response of plates to convected boundary layer turbulence is presented in Section 4.0, along with a summary of the necessary equations for joint-acceptance and deflection PSD. Using a digital computer program of these expressions, plate deflection spectra were computed for the predicted boundary layer turbulence and for variations in the space-correlation patterns associated with this turbulence. The results of these computations and an interpretive discussion are presented in Section 5.0. The primary results obtained are the relative response levels of the various modes for a given space correlation pattern, and the sensitivity of certain of the individual modal responses to longitudinal and lateral correlation lengths.

Pertinent conclusions obtained from the theoretical study and recommendations for further work in this problem area are discussed in Section 6.0.

2.0 VIBRATION CHARACTERISTICS OF IDEALIZED APOLLO SKIN STRUCTURE

In this section, the general configuration of the Apollo Spacecraft is presented showing the necessary geometry and dimensions. The skin panels of the SLA are shown in detail, as this structure is chosen for analysis as being representative of Apollo structure. The SLA shell is idealized to a uniform, flat, rectangular plate, simply supported along the four edges. The dynamic characteristics of this flat plate can be made approximately equivalent to those of the SLA by proper choice of the plate modes; and this choice is made so that the nodal pattern of the plate is similar to that of the SLA. A table of resonance frequencies for the plate is presented.

2.1 Idealization of SLA Structure to Dynamically Equivalent Flat Plate

A sketch of the Apollo Command Module, Service Module, and Spacecraft Lunar Excursion Module Adaptor (SLA) mounted on the Saturn launch vehicles is shown in Figure 2; and a more detailed sketch of the Apollo Spacecraft is shown in Figure 3. The section of the structure under study in this report is the skin of the SLA, which is shown in detail in Figures 4 and 5. (Figures 2 through 5 were extracted from Reference 6.)

Geometrically, the SLA is a truncated conical shell with a slant angle of slightly more than nine degrees. This shell is formed of two sets of panels, four panels per set. For this study, the vibration of the entire SLA is examined by considering the shell to be cut longitudinally, and when "unwrapped" to be approximately a rectangular panel. The upstream circumference is approximately 604 in. and the downstream circumference is approximately 816 in. The overall slant height of the SLA is 349 in. Therefore, the equivalent flat plate is assumed to have a length, along the flow axis, of 349 in., while the width of the plate is $(604 + 816)/2$ or 710 in. A diagram of this plate is shown in the following sketch.

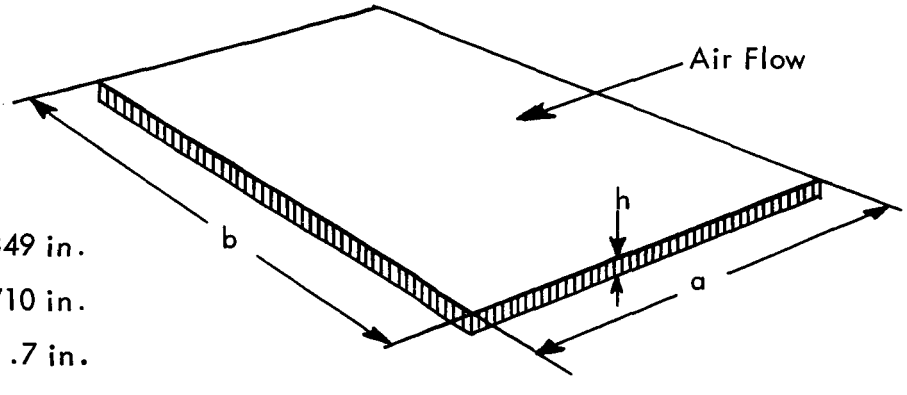

$a = 349$ in.

$b = 710$ in.

$h = 1.7$ in.

The skin is constructed from aluminum alloy (2024T-81) honeycomb material having an overall thickness of 1.7 in. and face sheet thicknesses of 0.015 in. and 0.032 in. The following sketch shows a typical cross-section of the honeycomb skin.

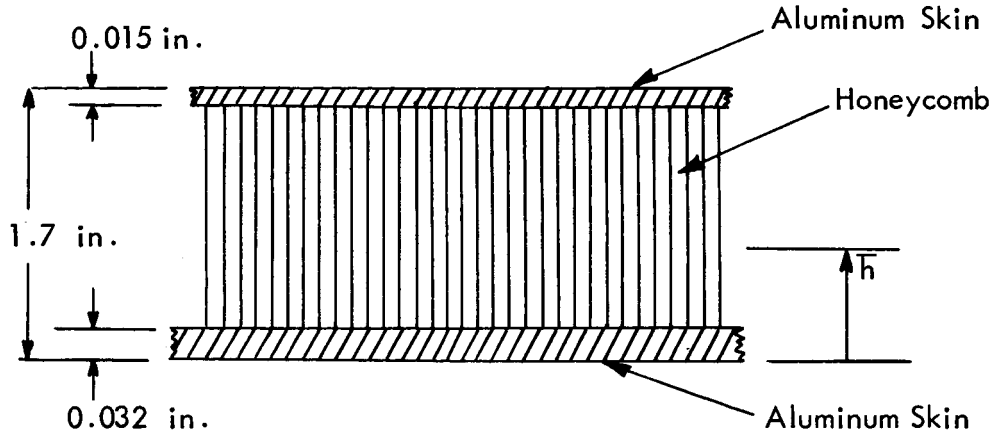

The location $\bar{h}$ of the neutral bending axis is easily obtained from the geometry of the above sketch, and is given by the equation

$$\bar{h} = \frac{(0.032)\cdot(0.16) + (0.015)\cdot(1.693)}{0.047}$$

$$= 0.551 \text{ in.}$$

The moment of inertia of cross-section area I about the neutral axis is given by:

$$I = (0.015)\cdot\left[\,1.693 - 0.551\,\right]^2 + (0.032)\left[0.535\right]^2$$

$$= 0.0287 \text{ in.}^3 \text{ (per unit length)}$$

From Reference 6, the mass/unit area μ of the material is approximately 2 lb./ft.^{2} or 0.0139 lb./in.^{2}

In an approximate manner, the modes of vibration of the SLA consist of two independent parts, namely, circumferential bending (ring) modes and longitudinal bending (beam) modes. These two components are shown diagrammatically in the sketch below for the fundamental SLA mode.

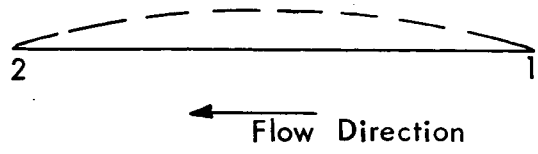

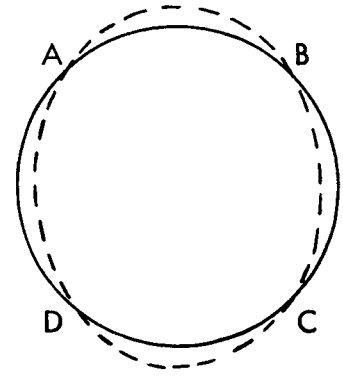

Longitudinal Beam Bending

Circumferential Ring Bending

For this mode, the equivalent mode of the flat plate is as shown below.

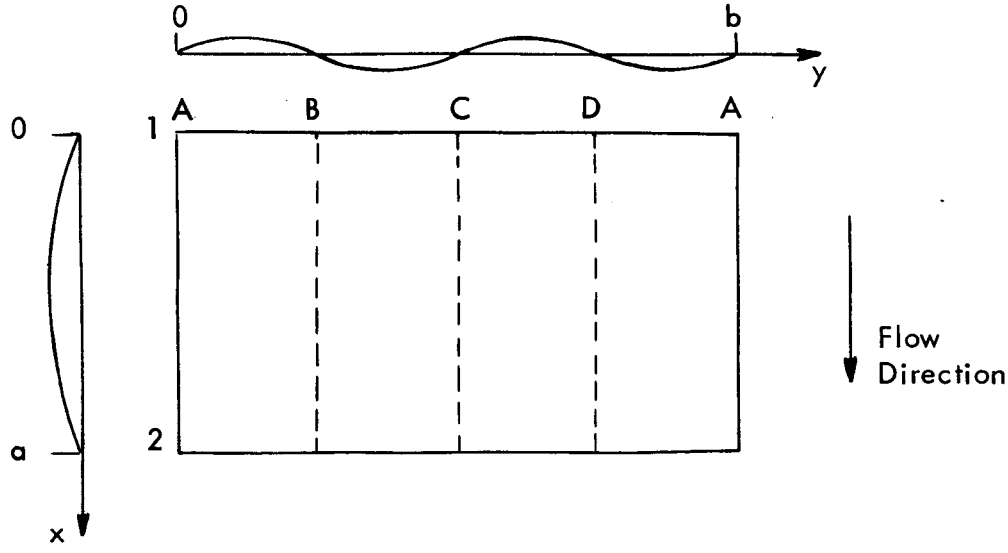

For a simply supported flat plate, this mode shape is given by the equation

$$\phi_{1,4}(x, y) = \sin(\pi \frac{x}{a}) \cdot \sin(4\pi \frac{y}{b}) \qquad (1)$$

For higher order modes of the plate, the mode shapes are

$$\phi_{m,n}(x, y) = \sin\left(m\pi \frac{x}{a}\right) \sin\left(n\pi \frac{y}{b}\right) \tag{2}$$

where

m = number of elastic half-waves along the x-axis

n = number of elastic half-waves along the y-axis.

Unlike a normal flat plate in which m and n can assume all integer values (m, n = 1, 2, 3, ...), the ring component of the SLA modes must have an even number of elastic half waves, which for dynamic similarity between SLA and plate requires that n must be even, starting with n = 4, so that n = 4, 6, 8, 10, ... The quantity m can assume all positive integer values.

Since the radius of curvature of the SLA shell is large compared with the shell thickness, effects of curvature on the resonance frequencies are neglected. Thus, the resonance frequency $f_{m,n}$ of the m n mode of the plate is given by the expression

$$f_{m,n} = \frac{1}{2\pi}\sqrt{\frac{EIg}{\mu}}\left[\left(\frac{m\pi}{a}\right)^2 + \left(\frac{n\pi}{b}\right)^2\right] \text{ cps} \tag{3}$$

where

E = Young's modulus of elasticity

= 10^7 lbs./in.^{2} for aluminum

I = Moment of inertia of cross-section area, per unit length

= 0.0287 in.^{3}

g = Acceleration of gravity

= 386.4 in./sec.^{2}

μ = Weight per unit area of plate, lb. /in.^{2}

= 0.0139 lb. /in.^{2}

a = Length of plate

= 349 in.

b = Width of plate

= 710 in.

Substituting these parameter values into (3) gives

$$f_{m,n} = 1.15\left[m^2 + 0.242\ n^2\right] , \quad \text{cps} \tag{4}$$

This frequency equation was numerically evaluated for:

m = 1, 2, 3, ..., 19, 20

n = 4, 6, 8, ..., 38, 40

and the results are presented in Table I.

The modal density of this plate can be readily determined from inspection of Table I. In the 5 - 10 cps band there are two resonances. In each 10 cps bandwidth, from 10 cps to 250 cps, there are four to eight resonances with an average of 5.7 modes per band in this range. In total, there are 139 modes within the frequency range from 5 cps to 250 cps.

3.0 THE TURBULENT PRESSURE FIELD ENVIRONMENT

In order to compute the power spectrum of the panel response to random pressure fluctuations, it is necessary to determine

i) The frequency spectrum of the forcing field,

ii) The overall level of the pressure fluctuations, and

iii) The longitudinal and lateral narrow band space correlations of the turbulent pressure field.

Since the Apollo capsule and SLA are in the wake flow from the escape tower, the boundary layer is thicker than would be normally expected, and it is found that the pressure fluctuations are increased in magnitude. Some areas of local separation are also probably caused by this wake flow.

Few flight measurements of pressure fluctuations have been made on the SLA. Thus the frequency spectrum is estimated from the nondimensional empirical curve given in Figure 6, extracted from Reference 4. This empirical curve was derived from measured data on several different missiles, including the Saturn I and is non-dimensionalized against vehicle diameter and free-stream velocity. In order to obtain a pressure power spectrum from Figure 7, it is necessary to choose representative values of the vehicle diameter D, free-stream velocity U, and an overall pressure level. The mean diameter for the SLA may be taken as $\bar{D} = (16.0 + 19.5)/2 = 17.8$ ft. The velocity at which maximum pressure fluctuations occur is approximately 1500 ft./sec. The overall sound pressure levels likely to be experienced by the SLA may be deduced from flight test data extrapolated from Saturn I flights (Reference 7). Unfortunately most of these data have been obtained for the Apollo sections immediately ahead of the SLA. Thus, use of the recommended testing levels given for these sections by Lowson, in Reference 7, are expected to be conservative by about 5 dB. Figures 7 and 8, from Reference 7, give the maximum pressure levels at any station versus Mach number. Using the data in Figures 7 and 8, and incorporating the 5 dB reduction factor, a reasonable pressure level for the SLA might be 160 dB. (It should be made clear that these levels are due to all sources such as wake flow, oscillating shocks, separated flows, and turbulent boundary layer pressure fluctuations). With $\bar{D} = 17.8$ ft., $U = 1500$ ft./sec., and an overall pressure level of 160 dB, the nondimensional empirical pressure spectrum in Figure 6 is converted to the true pressure spectrum shown in Figure 9. Both octave band and spectral density levels are presented.

It is much more difficult to predict the space correlations of the pressure field. Measurements in turbulent boundary layers at subsonic speeds are available; however, detailed measurements at supersonic speeds are very scarce and for separated flow, almost non-existent. In Figure 10, extracted from Reference 5, Maestrello

has shown that the measured narrow band longitudinal space correlation can be accurately represented by the empirical equation

$$R_p(\xi, 0, 0, \omega) = e^{-0.1(|\xi|\omega/U_c)} \cos(\xi\omega/U_c) \tag{5}$$

where ξ denotes separation distance $(x - x')$ along the flow axis, and U_c is the mean eddy convection velocity.

The pressure field is less correlated in the lateral than the longitudinal directions and the authors find that the equation

$$R_p(0, \zeta, 0, \omega) = e^{-2.0(|\zeta|\omega/U_c)} \cos(2.0\,\zeta\omega/U_c) \tag{6}$$

is a fairly good fit to Maestrello's experimental results. In (7), ζ denotes the lateral separation distance $(y - y')$. The product of these two results is used to give the spatial cross correlation:

$$R_p(\xi, \zeta, 0; \omega) = R_p(\xi, 0, 0; \omega) \cdot R_p(0, \zeta, 0; \omega) \tag{7}$$

The measurements made by Maestrello correspond to a Mach number of 0.52, while the Mach number range of interest for the SLA is $M = 0.8 \rightarrow 1.5$. Since no other measured space correlation data are available, it is necessary in this analysis to assume that (5) and (6) are valid for the higher Mach number range. Further, it should be noted that Maestrello's data are basically applicable to an attached turbulent boundary layer. Some of the flow over the SLA will undoubtedly be separated.

The mean velocity for convection of eddies downstream in the boundary layer was assumed to be 0.8 of the free stream velocity U. That is the convection velocity

$$U_c = 0.8\,U = 1200 \text{ ft./sec.}$$

With these uncertainties regarding the space correlation function, it is appropriate to determine the sensitivity of panel response to pressure correlation lengths in order to assess the validity of the computed results obtained in this report. Thus, the response calculations to be discussed in the remaining sections are made for a range of cross correlation lengths covering several orders of magnitude. Data are not readily available for correlation patterns in separated flow; however, it is expected that the pressure fluctuations will be more correlated.

4.0 METHOD OF ANALYSIS OF FLAT PLATE RESPONSE TO TURBULENCE

The equations necessary for the computations of the response of a flat plate to convected boundary layer turbulence are discussed in this section of the report. These equations can be found, in part, in Reference 3; however, for sake of completeness and to add to the clarity of the discussion, a brief derivation is presented herein. Expressions are obtained for the power spectral density of the deflection and acceleration; and, the complex expression for joint-acceptance, which contains typographical errors in Reference 3, is presented in its correct form without derivation. The greatest response of the plate, per unit input, is expected to occur at coincidence, where the convection velocity equals the bending wave propagation velocity; and special consideration is given to the response equations for this condition. Consideration is also given to the panel response in the two regimes above and below coincidence. At the lower resonance frequencies, the response occurs in discrete modes; and introducing realistic assumptions on the joint-acceptance, an approximate, simple expression is derived for the rms deflection of a single mode.

In the analysis to follow, the primary assumptions made are:

1.) the modes of vibration of the plate are uncoupled.

2.) the pressure field over the plate has a spectral density which is independent of position on the plate.

3.) the pressure field is homogeneous along the two principal axes of the plate so that the spatial correlation function along each axis is dependent only upon separation distance along that axis and independent of position along the axis.

4.) the space correlation function along each plate axis can be represented by an exponentially damped cosine.

5.) the response is a linear function of the excitation level.

6.) the resonance dynamic magnification factor is the same for all modes.

The geometry of the plate, the direction of the convected turbulent flow, and the pressure correlation pattern are shown in Figure 11.

4.1 Derivation of Equations for Response Spectral Density

With the assumption that the individual modes of the plate are uncoupled, each mode can be treated independently as a single degree of freedom system. In this sense, each mode will have an effective mass, a resonance frequency, and, for a given pressure distribution over the plate, each mode will have an effective or generalized force. For sinusoidal excitation of frequency ω, the steady state deflection, $W_{m,n}(x, y, t; \omega)$, at point (x, y) of the m,n mode is

$$W_{m,n}(x, y, t; \omega) = \phi_{m,n}(x, y) \cdot \frac{\mathcal{F}_{m,n}(t, \omega)}{\mathcal{K}_{m,n}} \cdot H(\omega/\omega_{m,n}) \cdot e^{i\theta(\omega)} \tag{8}$$

where

$\phi_{m,n}(x, y)$ = normalized (to unity) deflection shape of the m,n mode

= $\sin m\pi \frac{x}{a} \cdot \sin n\pi \frac{y}{b}$ for a simply-supported plate

$\mathcal{F}_{m,n}(t; \omega)$ = generalized force of the m,n mode

$$= \int_{x=0}^{a} \int_{y=0}^{b} P(x, y, t; \omega) \cdot \phi_{m,n}(x, y) \cdot dx\,dy, \text{ lb.} \tag{9}$$

$P(x, y, t; \omega)$ = sinusoidal pressure acting at point (x, y), lb./in.^{2}

$\mathcal{K}_{mn}$ = generalized stiffness of the m,n mode

$$= \mathcal{M}_{mn}\, \omega^2_{mn}/g, \text{ lb./in.} \tag{10}$$

$\mathcal{M}_{mn}$ = generalized weight of the mn mode

$$= \xi_{mn} M_o/g, \text{ lb.} \tag{11}$$

ξ_{mn} = generalized mass fraction of the mn mode

= $\frac{1}{4}$ for all modes of a simply-supported plate

M_o = total weight of panel, lb.

$$= ab\mu \tag{12}$$

a, b = edge dimensions of plate

μ = weight per unit area of plate, lb/in.^{2}

ω_{mn} = resonance frequency of the mn mode, rad./sec.

$H(\omega/\omega_{mn})$ = single degree of freedom dynamic magnification factor of the mn mode

$$= \left[\left\{ 1 - \left(\frac{\omega}{\omega_{mn}} \right) \right\}^2 + \frac{1}{Q^2} \left(\frac{\omega}{\omega_{mn}} \right)^2 \right]^{-1/2} \tag{13}$$

Q = dynamic magnification factor at resonance. (assumed to be equal for all modes)

$\theta(\omega)$ = phase angle between the pressure excitation and the response

$$= -\tan^{-1}\left[\frac{\frac{1}{Q}\left(\frac{\omega}{\omega_{mn}}\right)}{1-\left(\frac{\omega}{\omega_{mn}}\right)^2}\right] \tag{14}$$

The mean square value of the modal deflection in (8) is

$$\overline{W^2_{mn}(x, y, t; \omega)} = \frac{\phi^2_{mn}(x, y) \cdot H^2(\omega/\omega_{mn}) \cdot \overline{\mathcal{F}^2_{mn}(t; \omega)}}{\mathcal{K}^2_{mn}} \tag{15}$$

where the mean-square value of the generalized force is

$$\overline{\mathcal{F}^2_{mn}(t; \omega)} = \int_{x=0}^{a}\int_{y=0}^{b}\int_{x'=0}^{a}\int_{y'=0}^{b} \overline{P(x, y, t; \omega) \cdot P(x', y', t; \omega)} \cdot \phi_{mn}(x, y) \cdot \phi_{mn}(x', y')\, dx \cdot dy \tag{16}$$

If the applied pressures contain several discrete frequency components, then the total mean-square deflection due to all frequency components is the summation of the mean square deflection due to each frequency component. Further, if the frequency content of the fluctuating pressures is limited to a very narrow band, $\Delta\omega$, such that $\omega - \Delta\omega \leq \omega \leq \omega + \Delta\omega$, then the dynamic magnification factor $H(\omega/\omega_m)$ can be considered to be the same for all components in the $\Delta\omega$ band. Under this assumption, only the mean-square deflection

$$\overline{W^2_{mn}(x, y, t; \omega)}$$

and the pressure cross-correlation term

$$\overline{P(x, y, t; \omega)\ P(x', y', t; \omega)}$$

will vary with frequency in the band. Neglecting rigorous mathematical arguments, it is plausible that these two discrete frequency quantities can be replaced by their narrow band random equivalents which contain all frequency components in the $\Delta\omega$ band, their equivalents having the form

$$\overline{W^2_{mn}(x, y, t; \omega, \Delta\omega)}, \qquad \overline{P(x, y, t; \omega, \Delta\omega)\, P(x', y', t; \omega, \Delta\omega)}$$

Assuming next that the magnitudes of these quantities are proportional to $\Delta\omega$, so that spectral densities of each are certain to exist, then these narrow band quantities can be replaced by the deflection power spectral density $S_{w_{mn}}(x, y; \omega)$ and by the pressure cross power spectral density $S_p(x, y, x', y'; \omega)$ respectively. Thus, using (16), (15) can be rewritten in a form to give the deflection spectral density of the mn mode.

$$S_{w_{mn}}(x, y,; \omega) = \frac{\phi^2_{mn}(x, y) \cdot H^2(\omega/\omega_{mn})}{\mathcal{K}^2_{mn}} \cdot$$

$$\cdot \int_{x=0}^{a} \int_{y=0}^{b} \int_{x'=0}^{a} \int_{y'=0}^{b} S_p(x, y; x', y'; \omega)\, \phi_{mn}(x,y) \cdot \phi_{mn}(x',y') \cdot dx \cdot dy \cdot dx' \cdot dy' \tag{17}$$

It is convenient now to express the cross spectrum as the product of a pressure spectrum level $S_p(\omega)$ and a normalized (to unity) cross correlation function $R_p(x, y; x', y'; \omega)$ where it is assumed that the pressure spectrum level is uniform over the surface of the plate. Making this substitution in (17) and normalizing the range of integration gives

$$S_{w_{mn}}(x,y;\omega) = \frac{\phi^2_{mn}(x, y) \cdot H^2(\omega/\omega_{mn}) \cdot S_p(\omega) \cdot J^2_{mn}(\omega) \cdot a^2 \cdot b^2}{\mathcal{K}^2_{mn}} \tag{18}$$

where

$J^2_{mn}(\omega)$ = joint-acceptance of the mn mode

$$= \int_{x=0}^{1} \int_{y=0}^{1} \int_{x'=0}^{1} \int_{y'=0}^{1} R_p(x,y;x',y';\omega) \cdot \phi_{mn}(x,y) \cdot \phi_{mn}(x',y') \cdot dx \cdot dy \cdot dx' \cdot dy' \tag{19}$$

However, from (10), (11), and (12), the generalized stiffness $\mathcal{K}_{mn}$ is

$$\mathcal{K}_{mn} = \left(\frac{\mu}{g}\right) \cdot ab\ \xi_{mn}\ \omega^2_{mn}$$

so that (18) can be rewritten as

$$\frac{S_{w_{mn}}(x,y;\omega)}{S_p(\omega)} = \left(\frac{g}{\mu}\right)^2 \cdot \frac{\phi^2_{mn}(x,y) \cdot H^2(\omega/\omega_{mn}) \cdot J^2_{mn}(\omega)}{\xi^2_{mn}\ \omega^4_{mn}} \tag{20}$$

Summing expressions of the form (20) over all modes of the plate gives the total power spectral density of the plate deflection at point (x,y), namely

$$\boxed{\frac{S_w(x,y;\omega)}{S_p(\omega)} = \left(\frac{g}{\mu}\right)^2 \sum_{m,n} \frac{\phi^2_{mn}(x,y) \cdot H^2(\omega/\omega_{mn}) \cdot J^2_{mn}(\omega)}{\xi^2_{mn} \cdot \omega^4_{mn}}} \tag{21}$$

The power spectral density of acceleration response, $S_{\ddot{w}}(x, y; \omega)$ can be obtained from the corresponding deflection by the expression

$$S_{\ddot{w}}(x, y; \omega) = \omega^4 S_w(x, y; \omega)$$

so that

$$\frac{S_{ww}(x,y;\omega)}{S_p(\omega)} = \left(\frac{g}{\mu}\right)^2 \sum_{m,n} \left(\frac{\omega}{\omega_{mn}}\right)^4 \cdot \frac{\phi^2_{mn}(x,y) \cdot H^2(\omega/\omega_{mn}) \cdot J^2_{mn}(\omega)}{\xi^2_{mn}} \tag{22}$$

4.2 Joint - Acceptance for Convected Boundary Layer Turbulence

Introducing the assumption of homogeneity on the x and y components of the pressure field, the narrow band pressure space cross correlation function $R_p(x,y;x',y',\omega)$ appearing in (19), which is an even function, can be replaced by the simpler form

$$R_p(x,y,;x',y';\omega) = R_p(|\xi|, |\zeta|; \omega) \tag{23}$$

where

$$|\xi| = |x - x'|$$
$$|\zeta| = |y - y'|$$

so that the cross correlation, at a given frequency, is uniform over the plate and depends only upon the separation distances along the x and y axes.

From (5), (6), and (7), it is clear that (23) can be written in the functional form

$$R_p(x,y,;x',y';\omega) = e^{-\delta_x|\bar{\xi}|} \cos \gamma_x \bar{\xi} \cdot e^{-\delta_y|\bar{\zeta}|} \cos \gamma_y \bar{\zeta} \tag{24}$$

where, for a turbulent boundary layer

$$\left.\begin{aligned} \delta_x &= 0.10 \frac{\omega a}{U_c} & \delta_y &= 2 \frac{\omega b}{U_c} \\ \gamma_x &= \frac{\omega a}{U_c} & \gamma_y &= 2 \frac{\omega b}{U_c} \\ \bar{\xi} &= \xi/a = \bar{x} - \bar{x}' & \bar{\zeta} &= \zeta/b = \bar{y} - \bar{y}' \\ \bar{x} &= x/a & \bar{y} &= y/b \end{aligned}\right\} \tag{25}$$

When the mode shapes and expression (24) are substituted into (19), and the necessary integrations performed, Wilby, in Reference 3, shows that the expression for joint-acceptance of the mn mode of the plate becomes

$$J^2_{mn}(\omega) = 16\,\Phi_x\,\Phi_y / (mn\pi^2)^2$$

$$\Phi_x = \frac{1}{\Delta_x^2}\left\{p_x\left[1-(-1)^m\cdot e^{-\delta_x}\cdot\cos\gamma_x\right]+4(-1)^m q_x\cdot e^{-\delta_x}\cdot\sin\gamma_x+\frac{m\pi}{2}r_x\Delta_x\right\}$$

$$\Phi_y = \frac{1}{\Delta_y^2}\left\{p_y\left[1-(-1)^n\cdot e^{-\delta_y}\cdot\cos\gamma_y\right]+4(-1)^n q_y\cdot e^{-\delta_y}\cdot\sin\gamma_y+\frac{n\pi}{2}r_y\Delta_y\right\}$$

$$\Delta_x = \left[1+\left(\frac{\delta_x}{m\pi}\right)^2+\left(\frac{\gamma_x}{m\pi}\right)^2\right]^2-4\left(\frac{\gamma_x}{m\pi}\right)^2$$

$$\Delta_y = \left[1+\left(\frac{\delta_y}{n\pi}\right)^2+\left(\frac{\gamma_y}{n\pi}\right)^2\right]^2-4\left(\frac{\gamma_y}{n\pi}\right)^2$$

$$p_x = \left[1+\left(\frac{\delta_x}{m\pi}\right)^2-\left(\frac{\gamma_x}{m\pi}\right)^2\right]^2-4\left(\frac{\gamma_x}{m\pi}\right)^2\left(\frac{\delta_x}{m\pi}\right)^2$$

$$p_y = \left[1+\left(\frac{\delta_y}{n\pi}\right)^2-\left(\frac{\gamma_y}{n\pi}\right)^2\right]^2-4\left(\frac{\gamma_y}{n\pi}\right)^2\left(\frac{\delta_y}{n\pi}\right)^2$$

$$q_x = \left(\frac{\delta_x}{m\pi}\right)\left(\frac{\gamma_x}{m\pi}\right)\left[1+\left(\frac{\delta_x}{m\pi}\right)^2-\left(\frac{\gamma_x}{m\pi}\right)^2\right] \qquad (26)$$

$$q_y = \left(\frac{\delta_y}{n\pi}\right)\left(\frac{\gamma_y}{n\pi}\right)\left[1+\left(\frac{\delta_y}{n\pi}\right)^2-\left(\frac{\gamma_y}{n\pi}\right)^2\right]$$

$$r_x = \left(\frac{\delta_x}{m\pi}\right)\left[1+\left(\frac{\delta_x}{m\pi}\right)^2+\left(\frac{\gamma_x}{m\pi}\right)^2\right]$$

$$r_y = \left(\frac{\delta_y}{n\pi}\right)\left[1+\left(\frac{\delta_y}{n\pi}\right)^2+\left(\frac{\gamma_y}{n\pi}\right)^2\right]$$

For convenient reference later in the analysis, the joint-acceptance at the resonance frequency of each mode listed in Table I was numerically evaluated using a digital computer program of the equations (25) and (26). Values of $a = 349$ in, $b = 710$ in, and $U_c = 14{,}400$ in./sec. were used in the computations. The results are listed in Table I also.

In Reference (5), Maestrello's experimental data on lateral correlation of the turbulent boundary layer pressures shows no definite zero crossing; and thus, it might be sufficiently accurate to approximate (6) by an exponential function only. This is equivalent to setting $\gamma_y = 0$. Introducing this assumption into the joint-acceptance expression (26), the equations for Δ_y, p_y, q_y, r_y, and Φ_y simplify to the following:

$$\Delta_y = p_y = \left[1 + \left(\frac{\delta_y}{n\pi}\right)^2\right]^2$$

$$q_y = 0$$

$$r_y = \left(\frac{\delta_y}{n\pi}\right)\left[1 + \left(\frac{\delta_y}{n\pi}\right)^2\right]$$

and hence, noting from Section 2.0 that n is an even integer,

$$\Phi_y = \frac{1 - e^{-\delta_y}}{\left[1 + \left(\frac{\delta_y}{n\pi}\right)^2\right]^2} + \frac{\delta_y / 2}{\left[1 + \left(\frac{\delta_y}{n\pi}\right)^2\right]} \qquad (26a)$$

Exponential Lateral Correlation

4.3 Coincidence Conditions

Physically, the narrow band space correlation function $R_p(\xi, \zeta; \omega)$, is a measure of the time average value of the relative phase between pressures acting at two points (x,y) and (x', y') which are separated by component distances ξ and ζ. This implies that the pressure acting at any point (x', y') within the central region of positive correlation shown in Figure (11) will, over a long time average, be in-phase for an R_p fraction of this time with the pressure acting at the center (x, y) of the region. Thus, the central region of the positive correlation is often referred to as the correlation area, and its component dimensions as correlation lengths.

When the pressure correlation lengths are equal to the bending half-wave lengths of the plate for a particular mode, the pressures are, on the average, spatially correlated with the bending deflection shape of that mode. This condition results in a maximum joint-acceptance for the mode; and when this condition also occurs at or near the resonance frequency of the mode, the modal response is a maximum, thus producing what is commonly called coincidence. It can be shown that wave length matching at resonance for a finite plate causes the bending wave propagation velocity to be equal to the surface pressure convection velocity. The latter is often used as the basic definition of coincidence.

Because of the two-dimensional character of the plate mode shapes, it is possible to have coincidence along the two principle plate axes. All considerations of coincidence in this analysis are restricted, however, to the flow axis for the reasons that

a) simultaneous wave matching along two axes is unlikely,

b) the high rate of spatial decay of the lateral pressure correlation would minimize the effect of any such coincidence,

c) the lowest coincidence frequency occurs for the lowest order lateral deflection shape,

d) the coincident mode, or near coincident mode, corresponds to a large number m of elastic half waves.

If C_m denotes the bending wave velocity of the plate along the flow axis, and if U_c is the pressure convection velocity along this axis, then at coincidence,

$$U_c = C_m = \lambda_m f_m \tag{27}$$

where

λ_m = bending wave length of the m-th longitude mode of the plate

$$= 2a/m, \text{ in.} \tag{28}$$

f_m = resonance frequency of the m-th longitudinal mode of the plate, cps

$$= 1.15\, m^2 \quad \text{from (4)} \tag{29}$$

Combining (27), (28), and (29) gives the following approximate equation for the integer m, and the equation for the coincidence resonance frequency f_m:

$$m = \frac{U_c}{2.30a}$$

$$f_m = .217\left(\frac{U_c}{a}\right)^2$$

Coincidence Frequency (30)

With a convection velocity of $U_c = 14{,}400$ in./sec., and a plate length of $a = 349$ in., then the nearest integer m is $m = 18$ and the corresponding coincidence frequency $f_m = 360$ cps.

Consider next the joint-accpetance at resonance for the coincident mode. From (27) and (28), the coincident mode resonance frequency f_m is

$$f_m = \frac{m U_c}{2a} \quad \text{or} \quad \omega_m = \frac{m\pi U_c}{a} \tag{31}$$

Thus, from (25) and (31), the expressions for γ_x and δ_x are:

$$\gamma_x = m\pi$$

$$\delta_x = \frac{m\pi}{10}$$

Coincidence (32)

It is interesting to note that the coincidence value of $\gamma_x = m\pi$ ensures that the pressure correlation length is equal to a bending half-wave length of the coincident mode. Thus, this value is in agreement with the physical concept discussed above, where the maximum joint-acceptance is associated with maximum phase correlation between the pressure field and the mode shape. The proof is simple enough. From (24), the value of ξ $(= \xi_o)$ for the first zero crossing of the correlation function R_p along the flow axis is

$$\xi_o = a\,\bar{\xi}_o = \frac{\pi}{2}\cdot\frac{a}{\gamma_x} = \frac{a}{2m} \tag{33}$$

However, the pressure correlation length, ξ_c, along the flow axis is the distance between two successive zero crossings, so that

$$\xi_c = 2\,\xi_o = \frac{a}{m} = \text{length of bending half wave} \tag{34}$$

The joint-acceptance of the coincident mode at resonance can be obtained by substituting (32) into (26). For purposes of generality, γ_x is set equal to $m\pi$ in the substitution; however, the ratio $\delta_x/m\pi$, which is equal to 0.10 in (32), is set equal to an arbitrary, but small, parameter A so that

$$A \equiv \frac{\delta_x}{m\pi} \ll 1 \tag{35}$$

The advantage in this operation is to allow for simplification of the final result to pressure waves which have no longitudinal exponential spatial decay. Solving (26) for Δ_x, p_x, q_x, r_x, and Φ_x for this special coincidence case gives

$$\Delta_x = 4\left[1 + \frac{A^2}{2}\right]^2 - 4 \approx 4A^2$$

$$p_x = A^4 - 4A^2 \approx -4A^2$$

$$q_x = A^3$$

$$r_x = A(1 + A^2) \approx A$$

$$\Phi_x \approx \left[\frac{1}{16A^4} - 4A^2\left\{1 - e^{-m\pi A}\right\} + 4m\pi A^3\right]$$

or

$$\Phi_x = \frac{1}{4A^2}\left[-1 + e^{-m\pi A} + 4m\pi A\right] \quad \text{Coincidence} \tag{36}$$

If the pressure waves have no longitudinal decay in spatial correlation, similar to acoustic waves, the quantity A becomes zero and Φ_x reduces to

$$\Phi_x = \frac{(m\pi)^2}{8}$$

Coincidence for Non-decaying Longitudinal Pressure Field (37)

If the pressure field consists of plane acoustic waves propagating along the x-axis, the lateral correlation factor, $\exp(-\delta_y \bar{\zeta}) \cos \gamma_y \bar{\zeta}$, is equal to unity so that $\delta_y = \gamma_y = 0$. Inspection of (26) for Φ_y shows that for the modes of the plate considered in this analysis, ($n = 4, 6, 8, 10, \ldots$), $\Phi_y = 0$, and there is no other excitation, theoretically.

If the lateral component of the pressure field is coincident in the same manner as the longitudinal component of the pressure field, with no spatial decay in space correlation, then Φ_y is

$$\Phi_y = \frac{n\pi}{8}^2$$

Coincidence for Non-decaying Lateral Pressure Field (38)

In the case where both axes are simultaneously coincident with a non-decaying pressure correlation, (37) and (38) can be substituted into (26) to give the following

$$J^2_{mn}(\omega_{mn}) = \frac{1}{4}$$

Simultaneous Coincidence for the x and y axes for a Non-decaying Pressure Field (39)

It is interesting to note that this value of joint-acceptance is that given by Powell in Reference (8) for the case of perfect acoustic-bending wave length matching for a pinned-pinned beam.

More realistically, the joint - acceptance for the longitudinal coincident mode of the plate for actual homogeneous boundary layer turbulence, must be computed using (36) for Φ_x, and the general expression for Φ_y and J^2_{mn} in (26). A reasonably accurate simplification could be made in the expression for Φ_y by assuming that the lateral correlation function is non-periodic and exhibits only an exponential decay with distance ζ.

4.4 Response Below Coincidence

It was shown in Section 4.3 that $\gamma_x \equiv \omega a/U_c = m\pi$ and $\delta_x = \omega a/10\,U_c = m\pi/10$ correspond to longitudinal coincidence for the m-th longitudinal mode, the coincidence frequency being $\omega = \omega_m = m\pi U_c/a$. For a given mode m, values of the frequency $\omega < m\pi U_c/a$ are referred to as below coincidence frequencies; and modes having resonance frequency components $\omega_m < m\pi U_c/a$ are referred to as below coincidence modes. For these modes, the bending wave propagation velocity, C_m, is less than the turbulence pressure convection velocity U_c. This is easily shown by considering only the longitudinal component of the mode, for which the bending wave velocity is, by (28)

$$C_m = \lambda_m f_m$$

$$= 2\frac{a}{m}\cdot\frac{\omega_m}{2\pi} = \tag{40}$$

$$= \frac{a}{m}\cdot\frac{\omega_m}{\pi} < \frac{a}{m}\cdot\frac{mU_c}{a} = U_c$$

At resonance for the m-th longitudinal mode, the parameter γ_x is, using (40),

$$\gamma_x = \frac{\omega_m a}{U_c} = m\pi\left(\frac{C_m}{U_c}\right) \tag{41}$$

so that for modes which are below coincidence, $\gamma_x/m\pi < 1$. For those modes having resonance frequencies well below coincidence, $\gamma_x/m\pi \ll 1$, and the expressions (26) for the joint-acceptance amplify considerably. Noting from (25) that $\delta_x/m\pi \ll \gamma_x/m\pi \ll 1$, the quantities Δ_x, p_x, q_x, r_x, and Φ_x, become

$$\Delta_x \approx 1 - 2\left(\frac{\gamma_x}{m\pi}\right)^2$$

$$p_x \approx 1 - 2\left(\frac{\gamma_x}{m\pi}\right)^2$$

$$q_x \approx \left(\frac{\delta_x}{m\pi}\right)\left(\frac{\gamma_x}{m\pi}\right)$$

$$r_x \approx \left(\frac{\delta_x}{m\pi}\right)$$

and hence, retaining only first order terms so that $\Delta_x = p_x \approx 1$, $q_x \approx 0$, then

$$\Phi_x \approx 1 - (-1)^m e^{-\delta_x} \cos\gamma_x + \frac{\delta_x}{2} \qquad (42)$$

It is to be noted that this expression for Φ_x depends only upon whether m is an even or an odd integer. With $U_c = 14{,}400$ in./sec. and $a = 349$ in., the expressions (25) for γ_x and δ_x are

$$\gamma_x = \frac{\omega a}{U_c} = 0.152\ f$$

$$\delta_x = 0.10\,\frac{\omega a}{U_c} = 0.0152\ f \qquad (43)$$

A graph of (42) is presented in Figure 14 for a frequency range of 0 cps to 500 cps, for m equal to an even and an odd integer.

4.5 Response Above Coincidence

Above coincidence modes are those modes for which the bending wave velocity C_{mn} is greater than the pressure convection velocity, U_c. Thus, from (41) it is seen that at the resonance frequencies of such modes, having $\gamma_x/m\pi > 1$, and for

those modes having $\gamma_x/m\pi >> 1$, the joint-acceptance simplifies considerably. Noting that $\delta_x/m\pi << \gamma_x/m\pi$, the expressions (26) for Δ_x, p_x, q_x, r_x, and Φ_x reduce to the following:

$$\Delta_x \approx \left(\frac{\gamma_x}{m\pi}\right)^4 - 4\left(\frac{\gamma_x}{m\pi}\right)^2 \approx \left(\frac{\gamma_x}{m\pi}\right)^4$$

$$p_x \approx \left(\frac{\gamma_x}{m\pi}\right)^4$$

$$q_x \approx r_x \approx 0$$

so that Φ_x becomes

$$\Phi_x \approx \left(\frac{m\pi}{\gamma_x}\right)^4 \left[1 - (-1)^m \cdot e^{-\delta_x} \cdot \cos \gamma_x\right] \qquad (44)$$

which from (43) becomes

$$\Phi_x \approx \left(\frac{20.6\, m}{f}\right)^4 \left[1 - (-1)^m \cdot e^{-0.0152 f} \cdot \cos(0.152 f)\right] \qquad (45)$$

From (45), it is seen that Φ_x decreases with increasing frequency by the fourth power of frequency for a given mode m. This feature distinguishes the above coincident modes from the below coincident modes. Thus, the resonance excitation of the above coincidence modes decreases rapidly, as does the response.

4.6 Approximate Equation for RMS Deflection of a Single Mode

It is shown numerically in Section 5 that the joint-acceptance is a reasonably constant function of frequency over the response bandwidth, ω_{mn}/Q, for several of the modes. This fact can be used to obtain an approximate, yet convenient, expression for the rms deflection due to a single mode of vibration, if in addition, the reasonable assumption is made that the pressure spectral density $S_p(\omega)$ is also constant over the band. Replacing $J^2_{mn}(\omega)$ and $S_p(\omega)$ by their constant values $J^2_{mn}(\omega_{mn})$ and $S_p(\omega_{mn})$ respectively, and integrating the mn term of (21) from $f = 0$ to ∞ gives the mean-square value $W^2_{mn}(x, y; \omega)$ of the mn mode, namely

$$\overline{W^2_{mn}(x, y; \omega)} = \int_0^\infty S_w(x, y; \omega) \cdot df$$

$$\approx \left(\frac{g}{\mu}\right)^2 \frac{S_p(\omega_{mn}) \cdot \phi^2_{mn}(x,y) \cdot J^2_{mn}(\omega_{mn})}{2\pi \xi^2_{mn} \omega^3_{mn}} \int_0^\infty H^2\left(\frac{\omega}{\omega_{mn}}\right) \cdot d\left(\frac{\omega}{\omega_{mn}}\right)$$

However, it can be shown, using contour integration in the complex plane, that,

$$\int_0^\infty H^2\left(\frac{\omega}{\omega_{mn}}\right) \cdot d\left(\frac{\omega}{\omega_{mn}}\right) = \frac{\pi}{2} Q$$

Thus, the mean-square deflection of the mn mode is

$$\overline{W^2_{mn}(x, y; \omega)} \approx \left(\frac{g}{\mu}\right)^2 \cdot \frac{Q}{4} \cdot \frac{S_p(\omega_{mn}) \cdot \phi^2_{mn}(x,y) \cdot J^2_{mn}(\omega_{mn})}{\xi^2_{mn}\, \omega^3_{mn}} \tag{40}$$

The PSD of the deflection $S_w(x, y; \omega)$ at resonance for the mn mode can be obtained from (21) and is

$$S(x,y;\omega_{mn}) = \left(\frac{g}{\mu}\right)^2 \frac{S_p(\omega_{mn}) \cdot \phi^2_{mn}(x,y) \cdot Q \cdot J^2_{mn}(\omega_{mn})}{4\, \xi^2_{mn}\, \omega^3_{mn}} \cdot \frac{4Q}{\omega_{mn}} \tag{41}$$

From (40) and (41), the approximate mean-square response is given by the expression

$$\boxed{\overline{W^2_{mn}(x, y; \omega)} \approx \frac{\omega_{mn}}{4Q} \cdot S(x, y; \omega_{mn})} \tag{42}$$

5.0 COMPUTATION AND ANALYSIS OF RESPONSE

A digital computer program was made of the frequency equation (4), the deflection and acceleration response equations (21) and (22), and of the joint-acceptance equations (25) and (26). The program logic is presented in Appendix A. This program was first used to generate a summary list of the various plate resonance frequencies and joint-acceptance values given in Table I.

Ratios of the deflection and pressure power spectra were computed as functions of frequency for the points $x/a = 0.5$, $y/b = 0.125$, and $x/a = 0.25$, $y/b = 0.125$. These results are presented in Figures 15 through 17. An expanded frequency scale from $f = 0$ to 25 cps is used in Figure 15 in order to show the detailed nature of the modal deflection. This graph shows the essentially discrete modal character of the response frequency scales of $f = 0$ to 250 cps, which are used in Figures 16 and 17. These graphs show that the first mode, $(m,n) = (1,4)$ has the greatest deflection response per unit of pressure excitation, and that the deflections for higher modes drop off rapidly with increasing frequency. This rapid decrease in deflection PSD is due, in part, to the increasing stiffness of the plate with the order of the mode being excited, and hence with frequency; this stiffness being controlled by the quantity ω^4_{mn} appearing in equation (21). A curve of $1/\omega^4$ passing through the response peak of the (1, 4) mode is included in Figure 17 to show the general effect on the deflection of this increasing stiffness. The decreasing joint-acceptance, shown in Figure 12, is primarily responsible for the additional rate of decrease of response amplitude with frequency.

Using the equation (42) for the approximate mean-square deflection per mode, the rms deflections for the (1, 4), (1, 6), (2, 4), (3, 4), and (3, 6) modes were computed and the results are listed in Table II. The greatest rms deflection occurs for the (1, 4) mode, and this deflection (0.298 in.) is 17.5 % of the plate thickness of 1.7 inch.

The acceleration spectral density for the above two points on the plate are presented in Figures 18 and 19 for frequencies up to 250 cps. and 500 cps respectively. Figure 18 shows the essentially flat nature of the resonant acceleration response from 5 to 50 cps with a lower but flat response from 50 cps to 250 cps. Longitudinal coincidence of the plate was estimated in Section 4.3 to occur at about 375 cps, and for this reason the acceleration spectral density in Figure 19 is carried out to 500 cps so that the transition through and above coincidence is included. Figure 19 shows that above this predicted coincidence frequency, the response begins to drop off. This result is consistent with the decrease (by the fourth power of frequency) predicted in Section 4.5 for the above-coincidence modes.

In Section 4.5, it was assumed that the joint-acceptance is essentially constant over the frequency bond of the structural resonance. In support of this assumption for the highest response mode, the joint-acceptance for the (1, 4) mode is shown as a function of frequency in Figure 20. Clearly, $J^2_{14}(\omega)$ is nearly constant in the neighborhood of $f_{1,4} = 5.6$ cps.

In using Maestrello's pressure correlation data, it is recognized that these data were obtained for flow conditions which may be different from thosewhich occur in flight, so that the actual correlation lengths and spatial decay rates may differ from those employed in the above calculations. For this reason, it is desirable to test the sensitivity of the responses of the various modes to the correlation parameters. To do this, the following spatial correlation function was introduced into the computer program:

$$R_p(|\xi|,|\zeta|;\omega) = e^{-k_1\delta_x|\bar{\xi}|}\cos k_2\gamma_x\bar{\xi} \cdot e^{-k_3\delta_y|\bar{\zeta}|}\cos k_4\gamma_y\bar{\zeta} \qquad (43)$$

In the remaining Figures (21 through 29), the responses of the first few major modes are shown as functions of the constants k_1, k_2, k_3, and k_4.

In Figure 21, the resonant response of the (1, 4) mode is studied while the longitudinal correlation length parameter, k_2, is varied from 0 to 20, while the longitudinal pressure decay parameter, k_1, is given the discrete values k_1 = 0, 0.1, 1.0, 3.0, and 10.0. The axial correlation length, ξ_c, as a function of k_2, is

$$\xi_c = a\bar{\xi}_c = \frac{a\pi}{k_2\gamma_x} = \frac{\pi U_c}{\omega_{1,4}k_2} = \frac{U_c}{2k_2f_{1,4}}$$

which for U_c = 14,400 in./sec., $f_{1,4}$ = 5.6 cps gives

$$\xi_c = \frac{1290}{k_2} \text{ in.}$$

For k_2 = 1.0, the correlation length of 1290 inches is much greater than the panel length of 349 inches. Increasing k_2 decreases the correlation length; and as seen by Figure 21, this decreases the response of the fundamental mode. From the joint-acceptance curve given by Powell in Reference (8), it is expected that a minimum excitation of the (1, 4) mode will occur when the correlation length is only one-third the bending half wave length (349 in.) along the flow axis. A minimum response should occur, therefore, at k_2 = 1290/(349/) = 11.1, and this is seen to be the case in Figure 21.

The parameter k_1 controls the spatial correlation decay along the flow axis. For $k_1 = 0$, there is no correlation decay similar to the case of single frequency acoustic waves. For such excitation, cancellation between pressure and elastic waves due to wave mis-match, is sharper than for the exponentially decaying turbulent pressure field; and this is evidenced also in Figure 21.

The computer data presented in Figure 21 for the (1, 4) mode therefore shows certain distinct similarities to acoustic excitation as discussed by Powell in Reference (8), with the major difference coming from the exponential decay of the spatial correlation function. Further evidence of this can be found in Figures 22, for the (1, 6) mode, Figure 23 , for the (3, 4) mode, and Figure 24 for the (2, 4) mode.

It should be noted, however, that for the (1, 4) mode, the sensitivity of the response to changes in k_1 depends upon the value k_2, the greatest sensitivity occuring for $k_2 = 11$ and 18. For $k_2 = 1.0$, which was used in the analysis, Figure 21 shows that changes in $|\xi|$, should have only a slight effect on response. This is clearly in evidence in Figure 25, where $k_2 = k_3 = k_4 = 1.0$, and k_2 is varied.

The first negative peak of the longitudinal pressure correlation function occurs when

$$\bar{\xi} = \frac{\pi}{k_2 \gamma_x}$$

The value of the longitudinal correlation factor at this minimum is

$$e^{-k_1 \delta_x |\xi|} \cos k_2 \gamma_x \bar{\xi} = -e^{-\pi (k_1/k_2)(\delta_x/\gamma_x)}$$

$$= e^{-(\pi/10)(k_1/k_2)}$$

Thus, as the longitudinal correlation length is decreased by increases in the parameter k_2, the height of the negative correlation peak remains unchanged and equal to $\exp(-0.314)$, then $k_1 = k_2 = k$. The resulting changes in the response of the (1,4) mode with changes in k are quite different from those shown in Figure 21, as can be seen in Figure 26.

The sensitivity of the (1,4) mode to changes in the lateral correlation length and lateral correlation decay rate are shown in Figures 27 through 29. This sensitivity is not large when the lateral correlation lengths are decreased and when the decay rate is increased. However, if the lateral correlation pattern is altered in such a manner that the pressures tend to be correlated over greater lateral distances, the response level decreases sharply. This is expected since the lateral mode shape consists of an even number of elastic half-waves, giving rise to cancellation of the input over adjacent lateral half-waves.

6.0 CONCLUSIONS

A preliminary estimate has been made in this report of the vibration response charater-istics of SLA - like structure to convected boundary layer turbulence. The analysis is quite approximate in the sense that the SLA was represented as a simply supported, flat rectangular plate having the same cross-sectional dimensions and mass density as the SLA. The dynamic properties of the plate were made as equivalent to those of the SLA as could be done within this structural idalization by choosing only those resonance frequencies and modal patterns that are expected to occur on a pinned edge supported cylinder having a radius equal to the mean radius of the truncated conical SLA. All stiffness effects due to curvature were neglected. Further, approximations have been made regarding the uniformity of the SLA shell, the applicability of Maestrello's boundary layer correlation pattern to unsteady aero-dynamic flow during flight, linearity of the structure, and uniformity of the surface pressure field.

Within these limitations, the primary results obtained are:

1. The greatest response, per unit of pressure excitation level, occurs in the fundamental (1, 4) mode at 5.6 cps.

2. Certain higher order modes have response levels which are of the same order of magnitude as that of the fundamental mode; and when the pressure spectrum level is applied to the response spectral densities, higher order modes could dominate the response spectrum.

3. The average acceleration spectral density (taken about midway between the resonant peaks and antiresonant troughs) tends to be constant with frequency below the (bending velocity-convection velocity) coincidence, frequency, and to drop off sharply with frequency above coincidence.

4. No significant increase in acceleration spectral density occured at coincidence.

5. For nominal changes in the longitudinal pressure correlation pattern, the responses of the (1, 4) and (1, 6) modes experience little change, while the responses of the (3, 4) and (2, 4) modes could be significantly effected.

6. The general changes in the responses with changes in the pressure correlation pattern have strong resemblances to the sensitivity of panel vibrations to acoustic pressure correlations, although the sensitivity is much less for boundary layer turbulence.

7. For a spectral density level of 110 dB, at 5 to 6 cps, the fundamental mode of vibration rms response level is about 17.5 % of the thickness (1.7 inches) of the plate.

APPENDIX A

LOGIC FOR THE DIGITAL COMPUTER PROGRAM FOR STRUCTURAL RESPONSE TO BOUNDARY LAYER PRESSURE FLUCTUATIONS

A computer program was written to calculate the displacement power spectral density for the equivalent SLA panel as given by Equation (21). The flow chart is given in Table A 1, and the listing of the computer program is given in Table A 2. The modal contributions of the first 380 modes were calculated and summed to give the displacement spectral density for each point against frequency.

The program was modified slightly to give the effect upon the displacement for the first few resonances as various correlation parameters were varied.

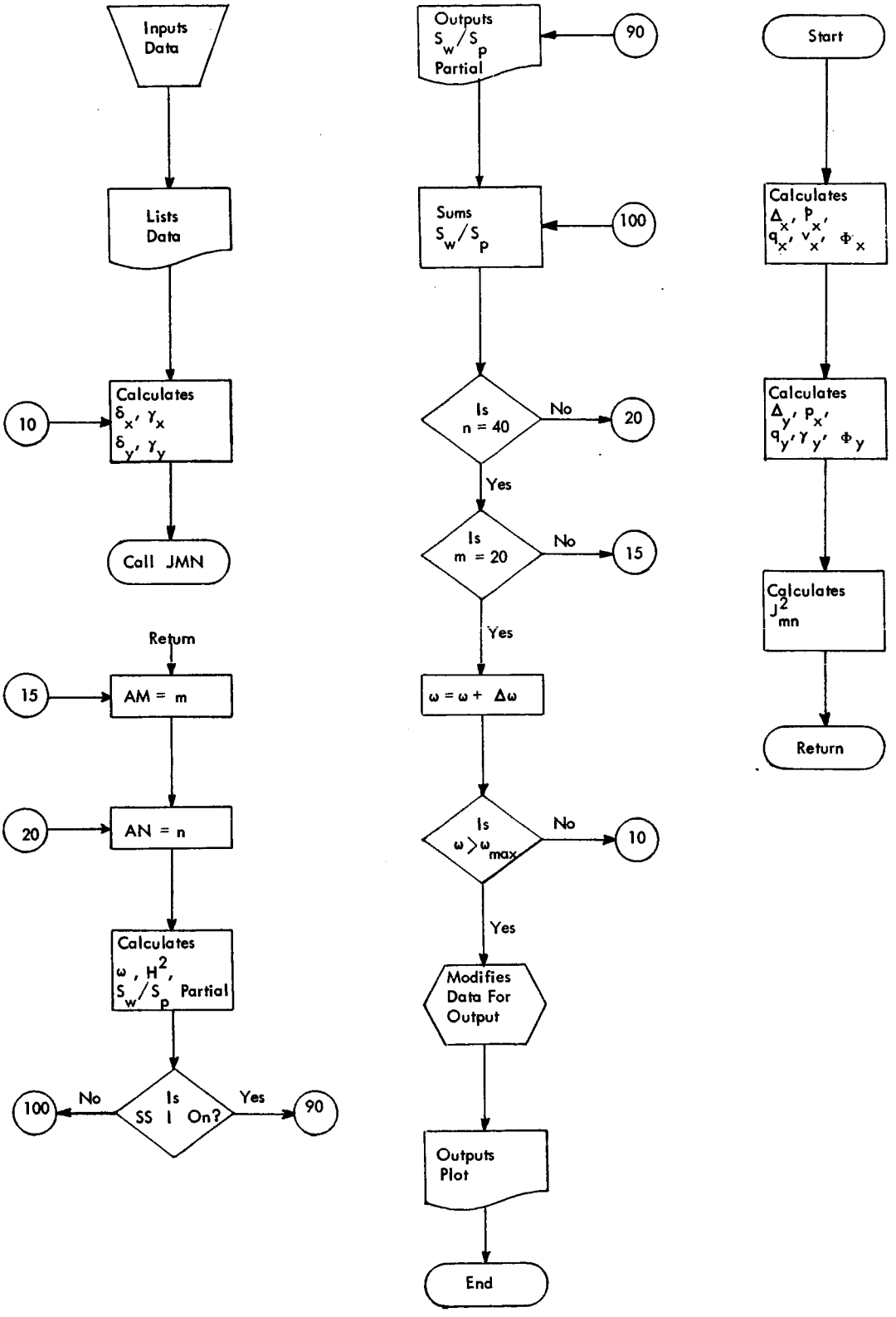

TABLE A 1. Flow Chart of Computer Program

```
                                    3200  FORTRAN     (2.1)              / /

      PROGRAM APOLLO2
C     RESPONSE OF SLA HONEYCOMB PANELS TO BOUNDARY LAYER NOISE
      DIMENSION SW(1800),OMA(1800)
      COMMON AJ(20,20),AX,AY,BX,BY,PD,H,PLX,PLY,X,Y
     1,M,N,E,PI,G,Q
      PI=3.14159265
      G=386.0
      E=1.0E+07
      READ(60,1001) M,N
      N=(N+2)/2
    1 READ(60,1000) UC,TMU,TI,X,Y,DOMA,OMAMAX,PLX,PLY,Q
      DOMA=DOMA*PI
      OMAMAX=OMAMAX*PI
      WRITE(61,1000)UC,TMU,TI,X,Y,DOMA,OMAMAX,PLX,PLY,Q
      OMA(1)=0.0
      K=0
   10 K=K+1
      AX=0.1*OMA(K)/UC
      BX=OMA(K)/UC
      AY=BY=2.0*BX
      CALL JMN
      SW(K)=0.0
      DO 100 I=1,M
      AM=FLOATF(I)
      DO 100 J=1,N
      AN=2.0+FLOATF(J*2)
      W=PI**2*((AM/PLX)**2+(AN/PLY)**2)*SQRTF(G*TI*E/TMU)
      PSI=SIN(AM*PI*X/PLX)*SIN(AN*PI*Y/PLY)
      H2=1.0/((1.0-(OMA(K)/W)**2)**2+(OMA(K)/W)**2/(Q**2))
      TEMP=G**2*PSI**2*AJ(I,J)*H2/(TMU**2*W**4*(1.0/4.0)**2)
      GO TO (90,100),SSWTCHF(1)
   90 WRITE(61,1002) TEMP,I,J
  100 SW(K)=SW(K)+TEMP
      OMA(K+1)=OMA(K)+DOMA
      IF(OMA(K).GT.OMAMAX)200,10
  200 CONTINUE
      DO 150 I=1,K
      OMA(I)=OMA(I)/196.5
  150 SW(I)=ALOG(SW(I)*1.0E+00)*.43429448
      WRITE(61,1003) SW(K),OMA(K)
      CALL PLOTCON
      CALL LOGAXIS(0.0,6.0,1.0,1.0,0)
      CALL REALAXIS(8.0,0.0,0.8,0.8,0)
      I=3
      DO 170 J=1,K
      CALL PLOT(OMA(J),SW(J),I)
  170 I=2
      CALL PLOT(0.0,0.0,-3)
      WRITE(59,1004)
      STOP
 1000 FORMAT(5E16.8)
 1001 FORMAT(5I3)
 1002 FORMAT(5X21HTHE VALUE OF WD/WP ISE16.8,8H, FOR M=I2,7H AND N=I2)
 1003 FORMAT(5X,6HSW/SP=E16.8,5X6HOMEGA=E16.8/)
 1004 FORMAT(5X,7HTHE END/)
      END

        3200 FORTRAN DIAGNOSTIC RESULTS - FOR   APOLLO2
```

TABLE A 2. The Listing of the Computer Program

```
                                        3200  FORTRAN     (2,1)                 / /
      SUBROUTINE JMN
      DIMENSION XX(20),YY(20)
      COMMON AJ(20,20),AX,AY,BX,BY,PD,H,PLX,PLY,X,Y
     1,M,N,E,PI,G,Q
      AXLX=AX*PLX
      BXLX=BX*PLX
      DO 10 I=1,M
      BOT=FLOATF(I)*PI
      A2=(AXLX/BOT)**2
      B2=(BXLX/BOT)**2
      DX=(1.0+A2+B2)**2-4.0*B2
      PX=(1.0+A2-B2)**2-4.0*A2*B2
      GX=(AXLX/BOT)*(BXLX/BOT)*(1.0+A2-B2)
      VX=AXLX/BOT*(1.0+A2+B2)
      GO TO (5,10),SSWTCHF(2)
    5 WRITE(61,1001) DX,PX,GX,VX,I
   10 XX(I)=1.0/(DX**2)*(PX*(1.0-(-1.0)**I*EXP(-AXLX)*COS(BXLX))
     1+4.0*GX*(-1.0)**I*EXP(-AXLX)*SIN(BXLX)+BOT/2.0*VX*DX)
      AYLY=AY*PLY
      BYLY=BY*PLY
      DO 20 I=1,N
      J=I*2+2
      BOT=(FLOATF(I*2)+2.0)*PI
      A2=(AYLY/BOT)**2
      B2=(BYLY/BOT)**2
      DY=(1.0+A2+B2)**2-4.0*B2
      PY=(1.0+A2-B2)**2-4.0*A2*B2
      GY=(AYLY/BOT)*(BYLY/BOT)*(1.0+A2-B2)
      VY=AYLY/BOT*(1.0+A2+B2)
      GO TO(15,20),SSWTCHF(2)
   15 WRITE(61,1000) DY,PY,GY,VY,I
   20 YY(I)=1.0/(DY**2)*(PY*(1.0-(-1.0)**J*EXP(-AYLY)*COS(BYLY))
     1+4.0*GY*(-1.0)**J*EXP(-AYLY)*SIN(BYLY)+BOT/2.0*VY*DY)
      DO 30 I=1,M
      AM=FLOATF(I)
      DO 30 J=1,N
      AN=FLOATF(J*2+2)
      AJ(I,J)=16.0*XX(I)*YY(J)/((AM*AN*PI**2)**2)
      GO TO (25,30),SSWTCHF(2)
   25 WRITE(61,1002) AJ(I,J),I,J
   30 CONTINUE
      RETURN
 1000 FORMAT(5X11HDY,PY,GY,VY/(4E16.8,I3))
 1001 FORMAT(5X11HDX,PX,GX,VX/(4E16.8,I3))
 1002 FORMAT(5X,12HJMN(OMA),I,J/(E16.8,2I3))
      END

        3200 FORTRAN DIAGNOSTIC RESULTS - FOR    JMN

NO ERRORS
```

TABLE A 2 (Continued)

```
      SUBROUTINE LOGAXIS(XLEN,YLEN,XSCALE,YSCALE,IEMP)
C     XLEN=DISTANCE FROM ORIGIN ALONG X-AXIS TO BE PLOTTED
C     YLEN=DISTANCE FROM ORIGIN ALONG Y-AXIS TO BE PLOTTED
C     XSCALE=LENGTH OF MAJOR DIVISION OF X-AXIS, NON-ZERO
C     YSCALE=LENGTH OF MAJOR DIVISION OF Y-AXIS, NON-ZERO
C     IEMP IS CODE WORD FOR PAGE TICS (IEMP=0 NOT DRAWN, =1 DRAWN)
C     SET PEN POINT AT LOCATION ORIGIN IS DESIRED
      DIMENSION TICK(9)
      IAX=9
      TICK(1)=.1458
      TICK(2)=.1969
      TICK(3)=.1549
      TICK(4)=.2218
      TICK(5)=.301
      TICK(6)=.3979
      TICK(7)=.6229
      TICK(8)=.699
 996  STOP=XLEN/XSCALE
      SIGN=1.
      IF(STOP .EQ. 0.)3,997
 997  ISTOP=IFIX(STOP)
      A=FLOATF(ISTOP)
      STOP=A*XSCALE
      IF(IEMP .EQ. 0)999,998
 998  CALL PLOT(0.,0.,-3)
      CALL PLOT(-1.5,0.,3)
      CALL PLOT(-1.5,0.,2)
      CALL PLOT(8.2,0.,3)
      CALL PLOT(8.5,0.,2)
      CALL PLOT(8.5,.2,1)
      CALL PLOT(-1.5,0.,3)
      CALL PLOT(-1.5,.2,2)
      CALL PLOT(0.,2.2,-3)
C     READY TO PLOT AXIS
C        MAKE SURE PEN POINT IS NOT DRIED UP
 999  CALL PLOT(0.,0.,-3)
      CALL PLOT(0.,0.,2)
      CALL PLOT(0.,0.,3)
      CALL PLOT(0.,0.,2)
      CALL PLOT(XLEN,0.,2)
      X=STOP
      DO 2 J=1,ISTOP
      CALL PLOT(X,.07,3)
      CALL PLOT(X,-.07,2)
      DO 1 I=1,IAX
      XD=X-(TICK(I)*XSCALE)
      CALL PLOT(XD,-.03,3)
 1    CALL PLOT(XD,.03,2)
 2    X=X-XSCALE
 3    CALL PLOT(0.,0.,3)
      CALL PLOT(0.,YLEN,2)
      STOP=YLEN/YSCALE
      IF(STOP .LT. 0.)4,5
 4    SIGN=-SIGN
```

TABLE A 2 (Continued)

```
5       IY=IFIX(STOP)
        IY=IABS(IY)
        A=FLOATF(IY)*SIGN
        STOP=YSCALE*A
        Y=STOP
        DO 7 I=1,IY
        CALL PLOT(.07,Y,3)
        CALL PLOT(-.07,Y,2)
        DO 6 J=1,IAX
        YD=Y-((TICK(J)*YSCALE)*SIGN)
        CALL PLOT(.03,YD,3)
6       CALL PLOT(-.03,YD,2)
7       Y=Y-(YSCALE*SIGN)
        CALL PLOT(0.,Y,3)
        RETURN
        ENTRY REALAXIS
        IAX=9
        TICK(1)=.1
        TICK(2)=.2
        TICK(3)=.5
        TICK(4)=.4
        TICK(5)=.5
        TICK(6)=.6
        TICK(7)=.7
        TICK(8)=.8
        TICK(9)=.9
        GO TO 996
        END

  3200 FORTRAN DIAGNOSTIC RESULTS - FOR   LOGAXIS


NO ERRORS
COMPASS ,X.
EQUIP,50=C1E1000
LOAD,56
RUN,10
```

TABLE A 2. (Continued)

APPENDIX B

BIBLIOGRAPHY

1. Richards, E.J. and Fahy, F.J., "Turbulent Boundary Layer Pressure Fluctuations over Two-Dimensional Surfaces and Narrow Delta Wings;" Acoustical Fatigue in Aerospace Structures, Edited by W.J. Trapp and D.M. Forney, Syracuse University Press, 1965

2. Ffowcs Williams, J.E., "Large Plate Response to Finite Mach Number Boundary Layer Flow", Acoustical Fatigue In Aerospace Structures, Edited by W.J. Trapp and D.M. Forney, Syracuse University Press, 1965

3. Lyon, R.H., "Boundary Layer Noise Response Simulation with a Sound Field", Acoustical Fatigue of Aerospace Structures, Edited by W.J. Trapp and D.M. Forney, Syracuse University Press, 1965

4. Wilby, J.F. and Richards, E.J., "Panel Response and Its Relation to the Type of Excitation", Acoustical Fatigue of Aerospace Structures, Edited by W.J. Trapp and D.M. Forney, Syracuse University Press, 1965

5. Fahy, F.J., "On Simulating the Transmission Through Structures of Noise from Turbulent Boundary Layer Pressure Fluctuations", J. Sound Vib. (1966) 3(1), 57 - 81

6. Bies, D.A., "A Wind Tunnel Investigation of Panel Response to Boundary Layer Pressure Fluctuations at Mach 1.4 and Mach 3.5", Bolt, Beranek, and Newman, Inc., Report No. 1264, Job No. 111722, Douglas Sub-contract DAC-A-64-432, NASA Prime Contract NASw-932, October 1965.

7. Tack, D.H., and Lambert, R.F., "Response of Bars and Plates to Boundary Layer Turbulence", Journal of the Aerospace Sciences, Vol. 29, pp 311 - 322, March 1962.

8. elBaroudi, M.Y., Ludwig, G.R., and Ribner, H.S., "An Experimental Investigation of Turbulence - Excited Panel Vibration and Noise (Boundary-Layer Noise)"NATO AFSOR 64-0590 Report 465, April 1963.

9. Ludwig, G.R., "An Experimental Investigation of the Sound Generated by Thin Steel Panels Excited by Turbulent Flow (Boundary Layer Noise)", University of Toronto UITA Report No. 87, November 1962.

10. elBaroudi, M. Y., "Turbulence -Induced Panel Vibration", University of Toronto UTIAS Report No. 98, February 1964.

11. Ribner, H.S., "The Noise of Aircraft", University of Toronto UTIAS Review No. 24, August 1964.

12. Ribner, H.S., "Boundary Layer Noise in the Interior of Aircraft", University of Toronto UTIA Report No. 37, April 1956.

13. Maestrello, L., "Measurement of Noise Radiated by Boundary Layer Excited Panels", J. Sound Vib. 2, 100, 1965.

14. Maestrello, L., "Measurement of Panel Response to Turbulent Boundary Layer Excitation", AIAA Journal, February 1965.

15. Powell, A., "On the Fatigue Failure of Structures due to Vibrations Excited by Random Pressure Fields", J. Acous. Soc. America, Vol. 30, 1130, 1958.

16. Bozich, D.J., "Spatial Correlation in Acoustic - Structural Coupling", J. Acous. Soc. America, Vol. 36, No. 1, January 1964.

REFERENCES

1. Crocker, M.J., "Final Report on Acoustic Qualification Test Plans for Saturn V S-IC Stage Structure", Wyle Laboratories Research Staff Technical Memorandum 65 - 17, September, 1965

2. Crocker, M.J., "Response of Panels to Oscillating Shock Waves", Wyle Laboratories Research Staff Report WR 66 - 17, March, 1966

3. Bull, M.K., Wilby, J.F., and Blackman, D.R., "Wall Pressure Fluctuations in Boundary Layer Flow and Response of Simple Structures to Random Pressure Fields", A.A.S.U. Report No. 243, University of Southampton, Department of Aeronautics and Astronautics, July, 1963

4. Lowson, M.V., "Prediction of the Inflight Fluctuating Pressures on Space Vehicles", Wyle Laboratories Research Staff Report WR 65 - 26, December, 1965

5. Maestrello, L., "Measurement and Analysis of the Response of Turbulent Boundary Layer Excited Panels", J. Sound Vib. (1965) 2 (3), 270 - 292

6. North American Aviation, Inc., "Structures and Mechanical Systems Course Number A - 512S", April 1, 1965

7. Lowson, M.V., "Prediction of Apollo Capsule Acoustic Environment", Private Communication, April, 1966

8. Powell, A., "Random Vibration", Vol. 1, Edited by Crandell, S.H., MIT Press, 1958, Chapter 8

ACKNOWLEDGEMENTS

The authors would like to thank Mr. P. Rhodes of the Wyle Computation Staff who wrote the computer program and the flow chart given in Appendix A.

f (m, n)cps	m	n	J^2_{mn}	f (m, n) cps	m	n	J^2_{mn}	f(m, n) cps	m	n	J^2_{mn}	f(m, n) cps	m	n	J^2_{mn}
9,6022	1	4	,05658525	9,0562	2	4	,01047542	14,8128	3	4	,00338428	22,8721	4	4	,00452179
11,1659	1	6	,03752970	14,6199	2	6	,01466803	20,3765	3	6	,00186335	28,4357	4	6	,00310248
18,9550	1	8	,02507504	22,4090	2	8	,01995709	28,1656	3	8	,00420350	36,2248	4	8	,00172908
28,9696	1	10	,01318003	32,4236	2	10	,02083051	38,1802	3	10	,00975527	46,2394	4	10	,00247818
41,2097	1	12	,00472521	44,6636	2	12	,01432975	50,4202	3	12	,01352759	58,4795	4	12	,00627684
55,6752	1	14	,00136957	59,1291	2	14	,00570255	64,8857	3	14	,01043329	72,9450	4	14	,00909118
72,3661	1	16	,00065312	75,8201	2	16	,00144767	81,5767	3	16	,00411664	89,6359	4	16	,00647637
91,2826	1	18	,00037475	94,7365	2	18	,00058929	100,4931	3	18	,00105711	108,5524	4	18	,00220837
112,4245	1	20	,00022681	115,8784	2	20	,00030572	121,6350	3	20	,00045871	129,6943	4	20	,00065941
135,7918	1	22	,00014851	139,2458	2	22	,00017951	145,0024	3	22	,00022823	153,0616	4	22	,00030813
161,3847	1	24	,00010134	164,8386	2	24	,00011402	170,5952	3	24	,00013646	178,6545	4	24	,00016375
189,2029	1	26	,00007153	192,6569	2	26	,00007767	198,4135	3	26	,00008704	206,4727	4	26	,00009875
219,2467	1	28	,00005205	222,7007	2	28	,00005496	228,4573	3	28	,00005934	236,5165	4	28	,00006499
251,5159	1	30	,00003878	254,9699	2	30	,00004021	260,7265	3	30	,00004241	268,7857	4	30	,00004511
286,0106	1	32	,00002950	289,4645	2	32	,00003023	295,2211	3	32	,00003134	303,2804	4	32	,00003265
322,7307	1	34	,00002284	326,1847	2	34	,00002322	331,9413	3	34	,00002378	340,0005	4	34	,00002443
361,6763	1	36	,00001797	365,1303	2	36	,00001816	370,8869	3	36	,00001844	378,9461	4	36	,00001876
402,8474	1	38	,00001433	406,3013	2	38	,00001443	412,0579	3	38	,00001456	420,1172	4	38	,00001471
446,2439	1	40	,00001158	449,6979	2	40	,00001162	455,4545	3	40	,00001167	463,5137	4	40	,00001173
33,2339	5	4	,00166840	45,8985	6	4	,00059498	60,8656	7	4	,00038829	78,1354	8	4	,00032506
38,7976	5	6	,00199448	51,4621	6	6	,00086190	66,4293	7	6	,00047244	83,6991	8	6	,00035386
46,5867	5	8	,00180147	59,2512	6	8	,00114845	74,2184	7	8	,00067724	91,4882	8	8	,00046930
56,6013	5	10	,00134105	69,2658	6	10	,00113428	84,2330	7	10	,00084709	101,5028	8	10	,00063050
68,8413	5	12	,00232675	81,5059	6	12	,00122992	96,4730	7	12	,00091407	113,7428	8	12	,00074472
83,3069	5	14	,00527642	95,9714	6	14	,00276694	110,9385	7	14	,00165343	128,2084	8	14	,00119747
99,9978	5	16	,00625831	112,6624	6	16	,00468958	127,6295	7	16	,00327437	144,8993	8	16	,00238959
118,9143	5	18	,00337261	131,5788	6	18	,00372040	146,5460	7	18	,00338713	163,8158	8	18	,00283792
140,0562	5	20	,00099832	152,7207	6	20	,00138753	167,6878	7	20	,00160935	184,9577	8	20	,00159981
163,4235	5	22	,00039840	176,0880	6	22	,00048281	191,0552	7	22	,00055306	208,3250	8	22	,00058534
189,0163	5	24	,00019412	201,6809	6	24	,00022617	216,6480	7	24	,00025119	233,9178	8	24	,00026213
216,8346	5	26	,00011231	229,4992	6	26	,00012469	244,4663	7	26	,00013348	261,7361	8	26	,00013729
246,8784	5	28	,00007088	259,5429	6	28	,00007601	274,5101	7	28	,00007972	291,7799	8	28	,00008127
279,1476	5	30	,00004782	291,8121	6	30	,00005021	306,7793	7	30	,00005187	324,0491	8	30	,00005242
313,6423	5	32	,00003397	326,3068	6	32	,00003510	341,2740	7	32	,00003581	358,5438	8	32	,00003593
350,3624	5	34	,00002507	363,0269	6	34	,00002559	377,9941	7	34	,00002585	395,2639	8	34	,00002578
389,3080	5	36	,00001906	401,9725	6	36	,00001927	416,9397	7	36	,00001933	434,2095	8	36	,00001919
430,4791	5	38	,00001483	443,1436	6	38	,00001489	458,1108	7	38	,00001485	475,3806	8	38	,00001469
473,8756	5	40	,00001176	486,5401	6	40	,00001175	501,5073	7	40	,00001167	518,7771	8	40	,00001152
97,7079	9	4	,00028078	119,5830	10	4	,00025303	143,7607	11	4	,00024574	170,2411	12	4	,00025992
103,2715	9	6	,00030391	125,1466	10	6	,00028152	149,3244	11	6	,00028060	175,8047	12	6	,00029869
111,0607	9	8	,00038345	132,9357	10	8	,00034988	157,1135	11	8	,00034477	183,5939	12	8	,00036025
121,0752	9	10	,00051024	142,9503	10	10	,00045297	167,1281	11	10	,00043573	193,6084	12	10	,00045396
133,3153	9	12	,00063824	155,1904	10	12	,00058588	179,3681	11	12	,00058524	205,8485	12	12	,00064030
147,7808	9	14	,00100505	169,6559	10	14	,00093848	193,8336	11	14	,00095072	220,3140	12	14	,00101059
164,4718	9	16	,00190417	186,3469	10	16	,00164704	210,5246	11	16	,00149843	237,0050	12	16	,00136963
183,3882	9	18	,00232947	205,2633	10	18	,00191241	229,4410	11	18	,00155522	255,9214	12	18	,00121988
204,5301	9	20	,00143044	226,4052	10	20	,00118768	250,5829	11	20	,00092828	277,0633	12	20	,00068682
227,8975	9	22	,00056548	249,7726	10	22	,00050264	273,9503	11	22	,00041787	300,4307	12	22	,00033053
253,4903	9	24	,00025681	275,3654	10	24	,00023708	299,5431	11	24	,00020761	326,0235	12	24	,00017410
281,3086	9	26	,00013529	303,1837	10	26	,00012767	327,3614	11	26	,00011569	353,8418	12	26	,00010117
311,3523	9	28	,00008020	333,2274	10	28	,00007655	357,4051	11	28	,00007077	383,8855	12	28	,00006358
343,6215	9	30	,00005168	365,4966	10	30	,00004963	389,6744	11	30	,00004648	416,1547	12	30	,00004253
378,1162	9	32	,00003535	399,9913	10	32	,00003409	424,1690	11	32	,00003221	450,6494	12	32	,00002985
414,8364	9	34	,00002533	436,7114	10	34	,00002448	460,8892	11	34	,00002327	487,3695	12	34	,00002177
453,7820	9	36	,00001882	475,6570	10	36	,00001821	499,8348	11	36	,00001739	524,3151	12	36	,00001639
494,9530	9	38	,00001439	516,8281	10	38	,00001394	541,0058	11	38	,00001336	567,4862	12	38	,00001265
538,3495	9	40	,00001127	560,2246	10	40	,00001092	584,4024	11	40	,00001049	610,8827	12	40	,00000998

TABLE 1. Values of First 380 Resonance Frequencies of Plate and Joint-Acceptance For Each Frequency

f (m, n) cps	m	n	J^2_{mn}	f (m, n) cps	m	n	J^2_{mn}	f (m, n) cps	m	n	J^2_{mn}	f (m, n) cps	m	n	J^2_{mn}
199,0241	13	4	,00029333	230,1097	14	4	,00034732	263,4980	15	4	,00044406	299,1890	16	4	,00059595
204,5877	13	6	,00033405	235,6734	14	6	,00039690	269,0617	15	6	,00051443	304,7526	16	6	,00066786
212,3769	13	8	,00040042	243,4625	14	8	,00048650	276,8508	15	8	,00062976	312,5417	16	8	,00075305
222,3914	13	10	,00051996	253,4771	14	10	,00064461	286,8654	15	10	,00078264	322,5563	16	10	,00080761
234,6315	13	12	,00074941	265,7171	14	12	,00087092	299,1054	15	12	,00090387	334,7964	16	12	,00076642
249,0970	13	14	,00106606	280,1827	14	14	,00103733	313,5709	15	14	,00086898	349,2619	16	14	,00060804
265,7880	13	16	,00119126	296,8736	14	16	,00093648	330,2619	15	16	,00064858	365,9529	16	16	,00040738
284,7044	13	18	,00089689	315,7901	14	18	,00061130	349,1784	15	18	,00039533	384,8693	16	18	,00025322
305,8463	13	20	,00048606	336,9320	14	20	,00033557	370,3203	15	20	,00023008	406,0112	16	20	,00015808
329,2137	13	22	,00025235	360,2993	14	22	,00018810	393,6876	15	22	,00013851	429,3785	16	22	,00010183
354,8065	13	24	,00014135	385,8921	14	24	,00011224	419,2804	15	24	,00008781	454,9714	16	24	,00006814
382,6248	13	26	,00008591	413,7104	14	26	,00007137	447,0987	15	26	,00005840	482,7897	16	26	,00004730
412,6685	13	28	,00005574	443,7542	14	28	,00004789	477,1425	15	28	,00004051	512,8334	16	28	,00003391
444,9377	13	30	,00003811	476,0234	14	30	,00003356	509,4117	15	30	,00002913	545,1026	16	30	,00002501
479,4324	13	32	,00002719	510,5181	14	32	,00002438	543,9064	15	32	,00002159	579,5973	16	32	,00001891
516,1526	13	34	,00002007	547,2382	14	34	,00001826	580,6265	15	34	,00001641	616,3174	16	34	,00001461
555,0982	13	36	,00001524	586,1838	14	36	,00001402	619,5721	15	36	,00001275	655,2630	16	36	,00001150
596,2692	13	38	,00001185	627,3549	14	38	,00001099	660,7432	15	38	,00001010	696,4341	16	38	,00000921
639,6657	13	40	,00000940	670,7514	14	40	,00000878	704,1397	15	40	,00000813	739,8306	16	40	,00000748
337,1825	17	4	,00069978	377,4788	18	4	,00060692	420,0776	19	4	,00038841	464,9791	20	4	,00021799
342,7462	17	6	,00071854	383,0424	18	6	,00056761	425,6413	19	6	,00034561	470,5428	20	6	,00019432
350,5353	17	8	,00070981	390,8315	18	8	,00049984	433,4304	19	8	,00029149	478,3319	20	8	,00016617
360,5499	17	10	,00064515	400,8461	18	10	,00040744	443,4450	19	10	,00023388	488,3465	20	10	,00013712
372,7899	17	12	,00052026	413,0862	18	12	,00030816	455,6850	19	12	,00018047	500,5865	20	12	,00011007
387,2555	17	14	,00037268	427,5517	18	14	,00022168	470,1505	19	14	,00013572	515,0520	20	14	,00008673
403,9464	17	16	,00024942	444,2426	18	16	,00015593	486,8415	19	16	,00010082	531,7430	20	16	,00006761
422,8629	17	18	,00016452	463,1591	18	18	,00010939	505,7579	19	18	,00007477	550,6594	20	18	,00005250
444,0048	17	20	,00010982	484,3010	18	20	,00007754	526,8998	19	20	,00005574	571,8013	20	20	,00004081
467,3721	17	22	,00007512	507,6683	18	22	,00005585	550,2672	19	22	,00004195	595,1687	20	22	,00003188
492,9649	17	24	,00005279	533,2612	18	24	,00004097	575,8600	19	24	,00003194	620,7615	20	24	,00002507
520,7832	17	26	,00003809	561,0794	18	26	,00003062	603,6783	19	26	,00002464	648,5798	20	26	,00001988
550,8270	17	28	,00002817	591,1232	18	28	,00002331	633,7221	19	28	,00001925	678,6236	20	28	,00001591
583,0962	17	30	,00002130	623,3924	18	30	,00001805	665,9913	19	30	,00001524	710,8928	20	30	,00001285
617,5909	17	32	,00001643	657,8871	18	32	,00001419	700,4859	19	32	,00001221	745,3874	20	32	,00001048
654,3110	17	34	,00001290	694,6072	18	34	,00001133	737,2061	19	34	,00000990	782,1076	20	34	,00000862
693,2566	17	36	,00001030	733,5528	18	36	,00000916	776,1517	19	36	,00000811	821,0532	20	36	,00000716
734,4277	17	38	,00000833	774,7239	18	38	,00000750	817,3227	19	38	,00000671	862,2242	20	38	,00000599
777,8242	17	40	,00000683	818,1204	18	40	,00000620	860,7193	19	40	,00000561	905,6208	20	40	,00000505

TABLE 1 (Concluded)

Mode	Frequency f cps	Plate Pos.^{n} x ; y	S_w/S_p $in.^2/(psi)^2$	S_p dB; $(psi)^2/$ cps	W^2_{mn} * $in.^2$	W_{mn} rms in.
1, 4	5.6022	a/2 ; b/8	3.0×10^{5}	110; 8.4×10^{-7}	0.0889	0.298
1, 6	11.1659	a/2 ; b/8	6.2×10^{3}	121; 1.06×10^{-5}	0.0461	0.215
3, 4	14.8128	a/2 ; b/8	4.0×10^{2}	123; 1.5×10^{-5}	0.00558	0.075
3, 6	20.3765	a/2 ; b/8	3.2×10^{1}	124; 2.02×10^{-5}	0.000826	0.029
2, 4	9.0562	a/4 ; b/8	7.5×10^{3}	120; 8.4×10^{-6}	0.0360	0.19

* $$W^2_{mn} = \frac{\omega_{mn}}{4Q}\left(\frac{S_w}{S_p}\right) S_p$$

Overall rms displacement (For $x = a/2$; $y = b/8$)

$$W_o \approx 0.41 \text{ in.}$$

TABLE 2. Calculated RMS Deflections for the Dominant Plate Modes

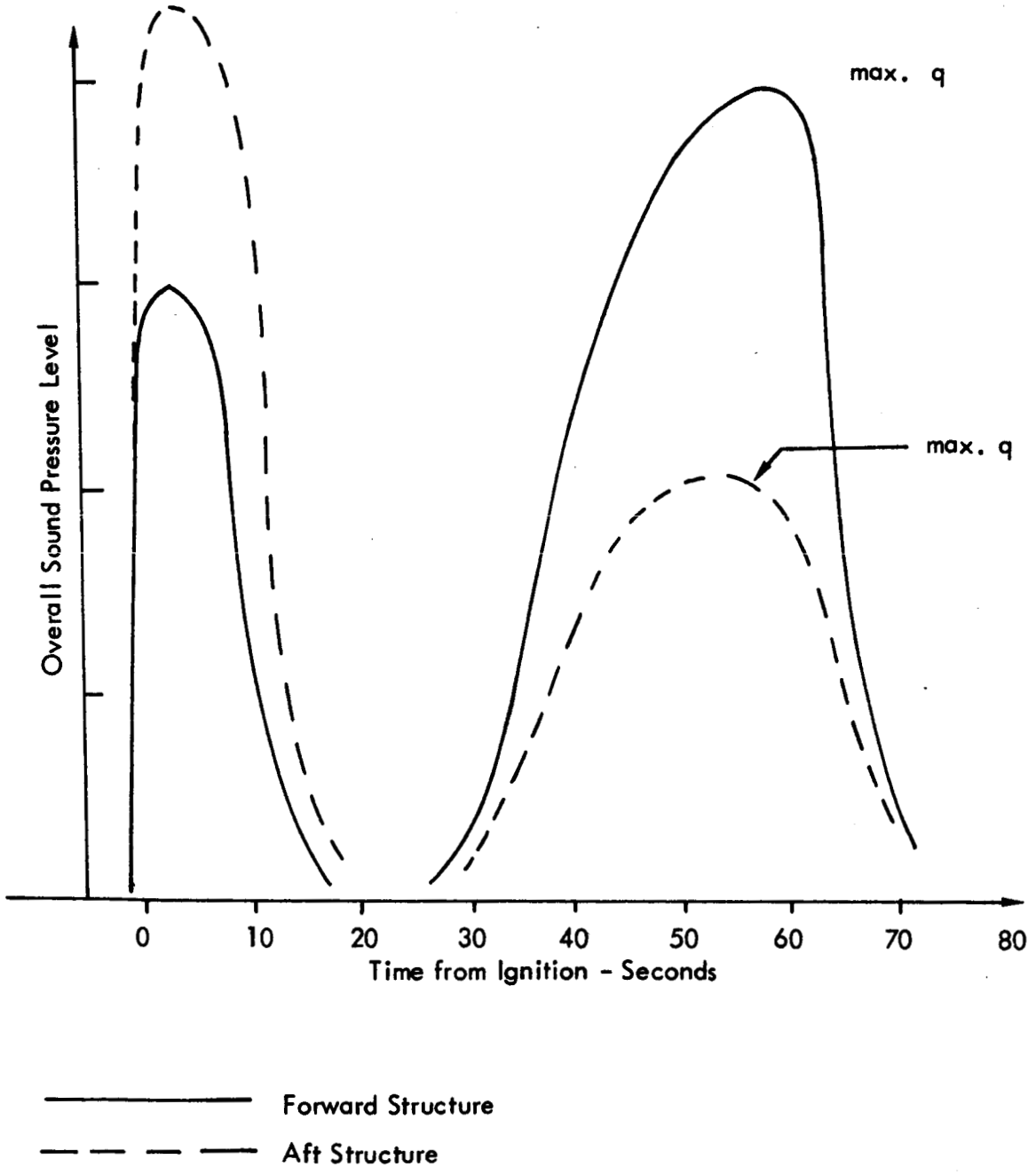

Figure 1: Typical Overall SPL Time Histories Experienced on Large Rocket Vehicles (From Reference 1).

SATURN APOLLO LAUNCH VEHICLE CONFIGURATIONS

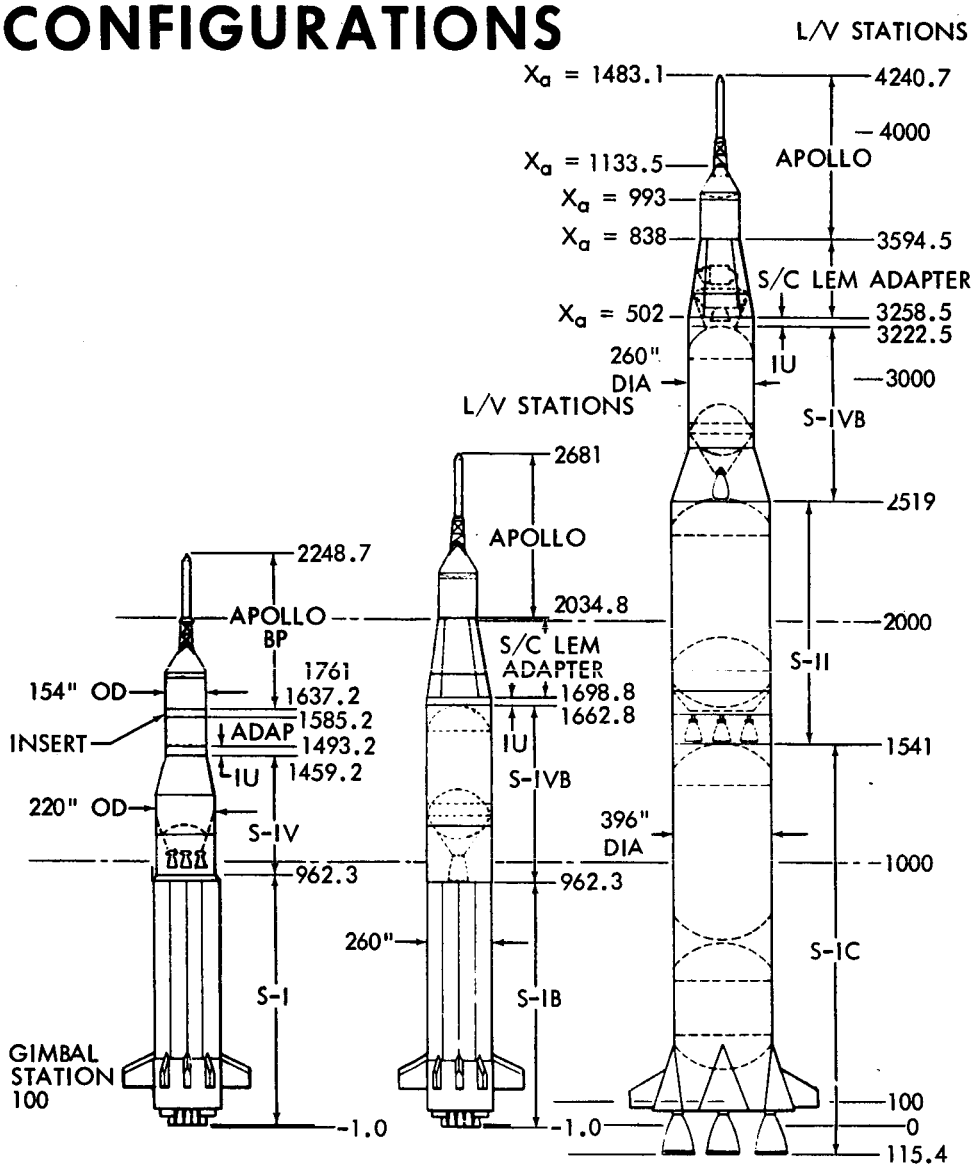

Figure 2. Saturn Launch Vehicles with Apollo Spacecraft
(Extracted from Reference 6)

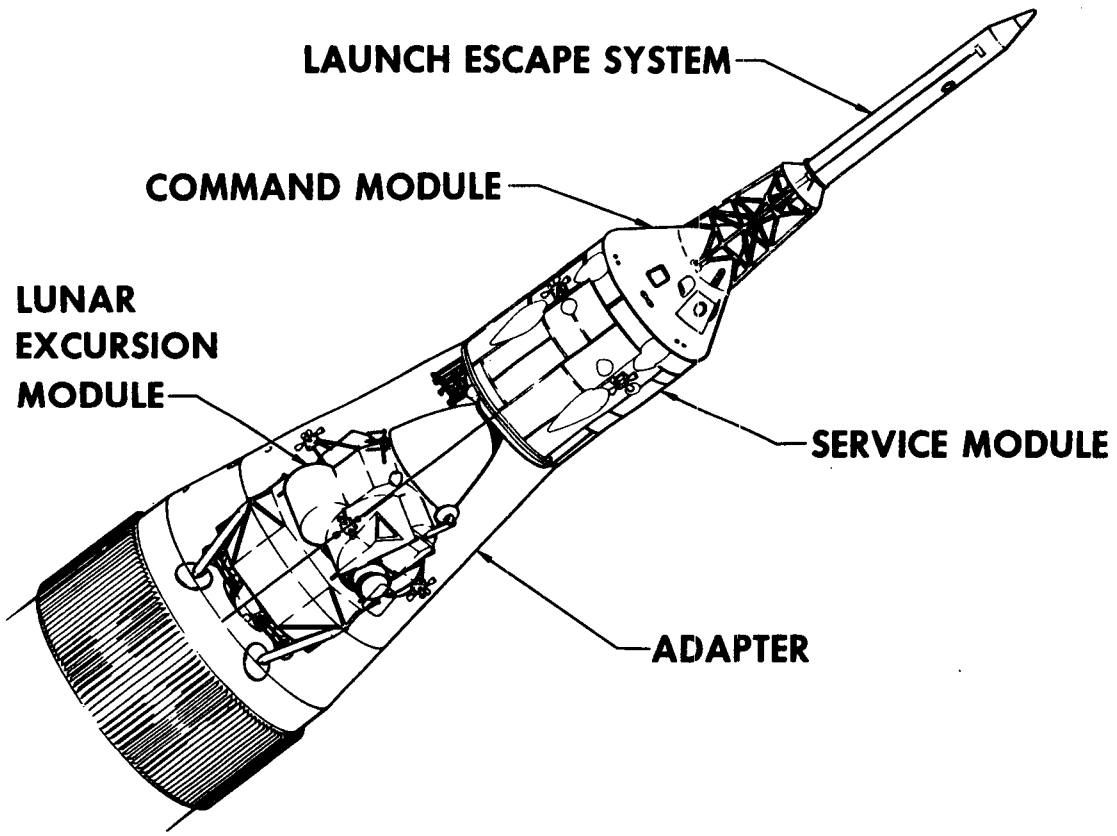

Figure 3. Details of Apollo Command Module, Service Module and LEM Adapter (Extracted from Reference 6)

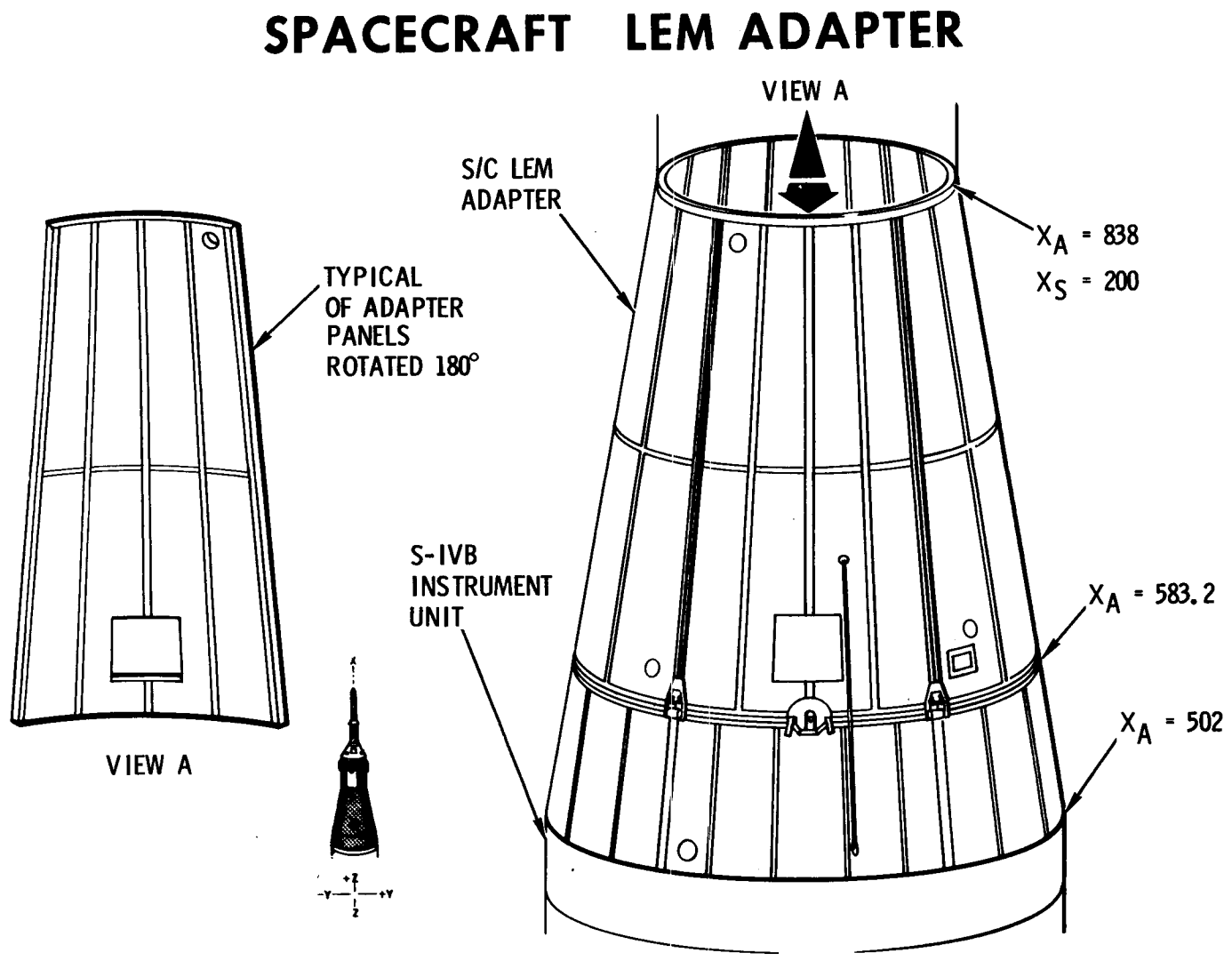

Figure 4. General Configuration of SLA Skin Structure (Extracted from Reference 6)

ADAPTER PANEL SEPARATION LINE

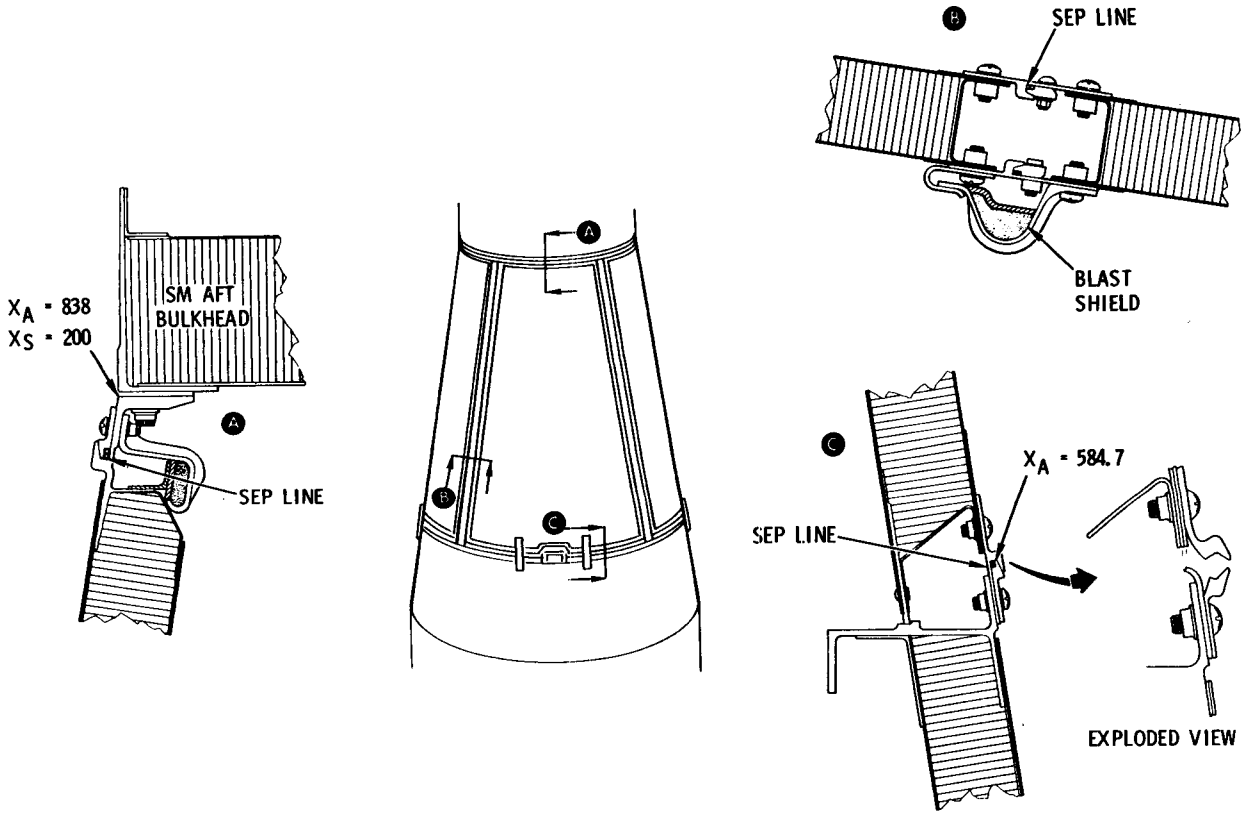

Figure 5. Details of SLA Honeycomb Skin Construction (Extracted from Reference 6)

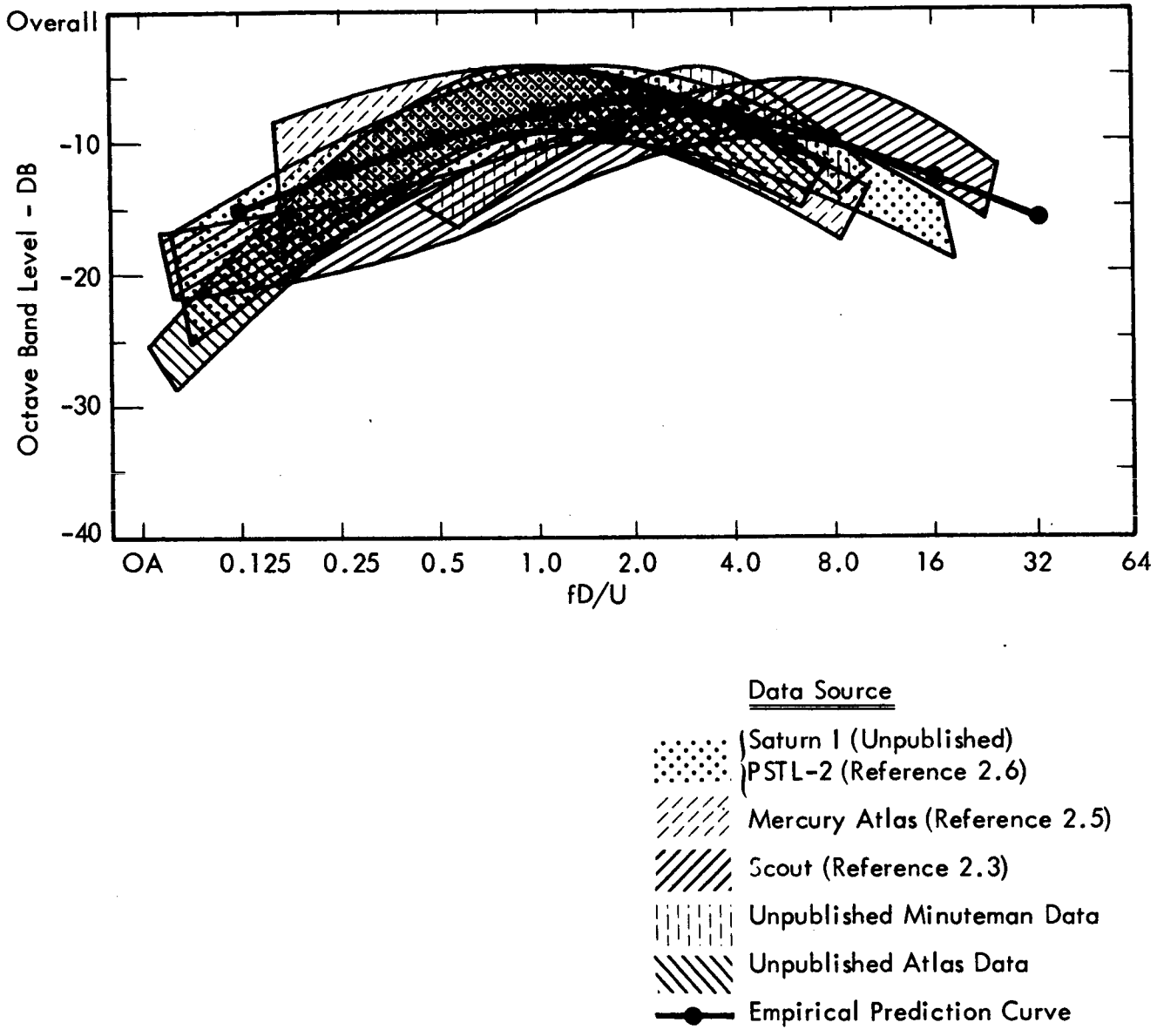

Figure 6. Non-Dimensionalized Fluctuating Pressure Spectra For a Number of Launch Vehicles (Extracted from Reference 4.)

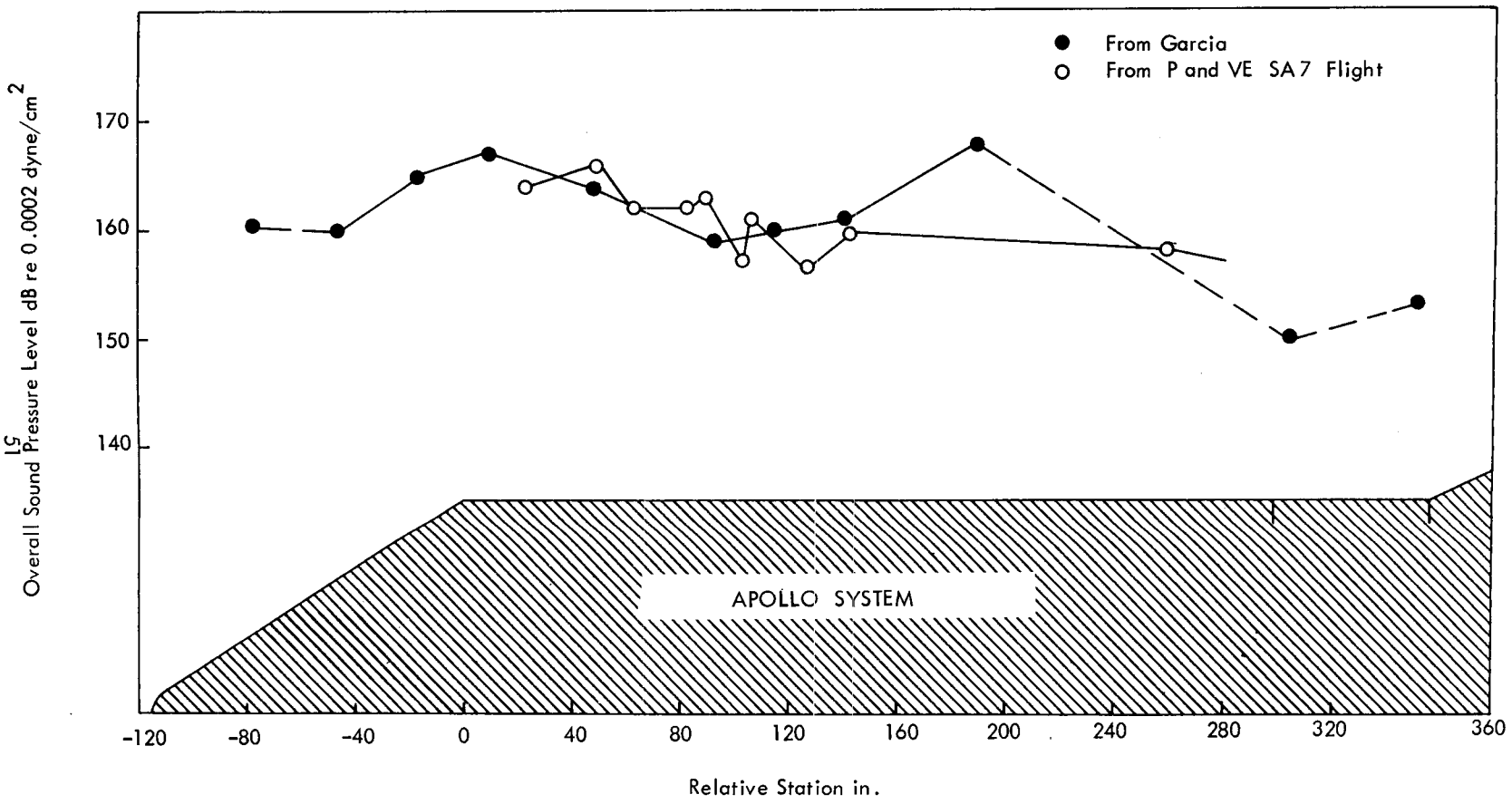

Figure 7. Maximum Fluctuation at any Mach Number versus Station.

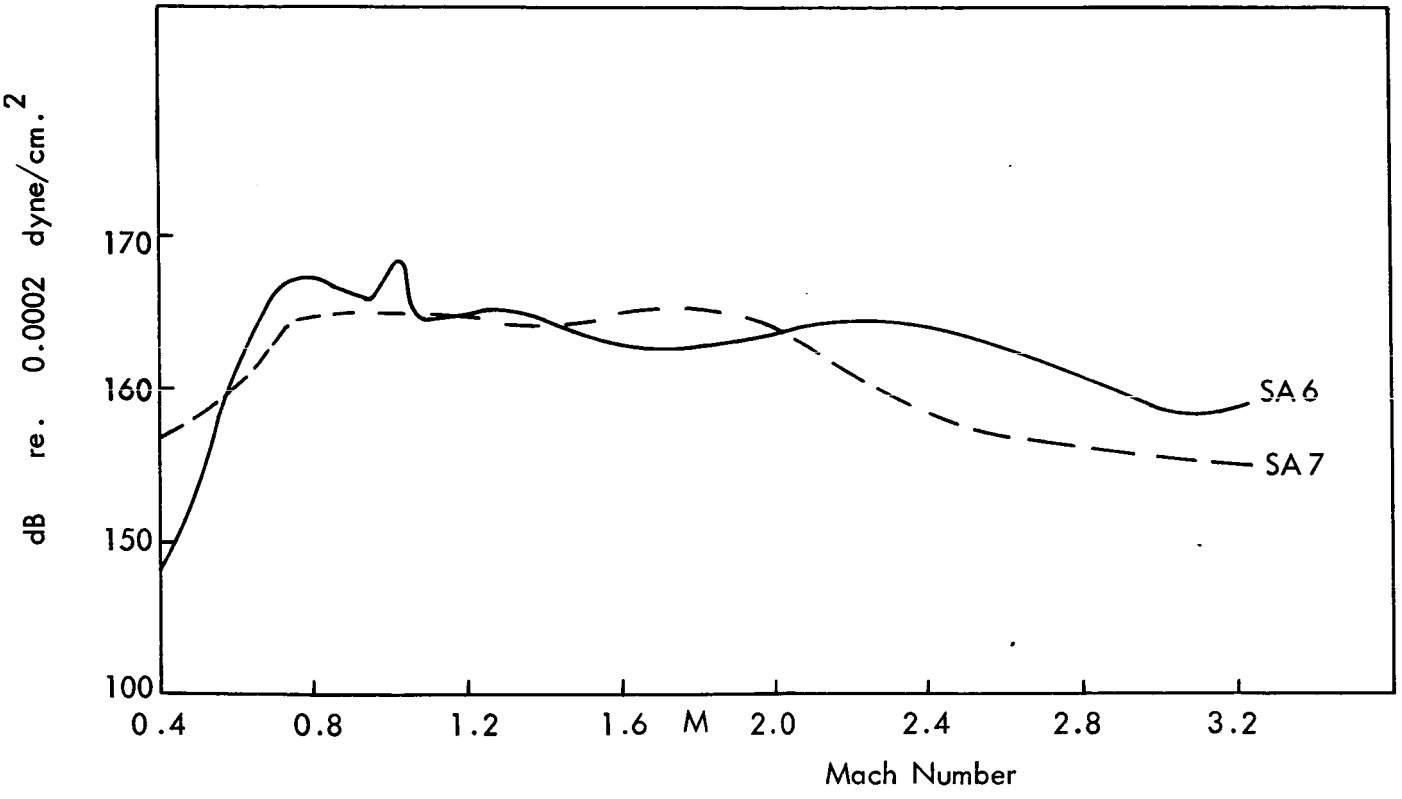

Figure 8. Envelope of Maximum Fluctuation at any Station versus Mach Number

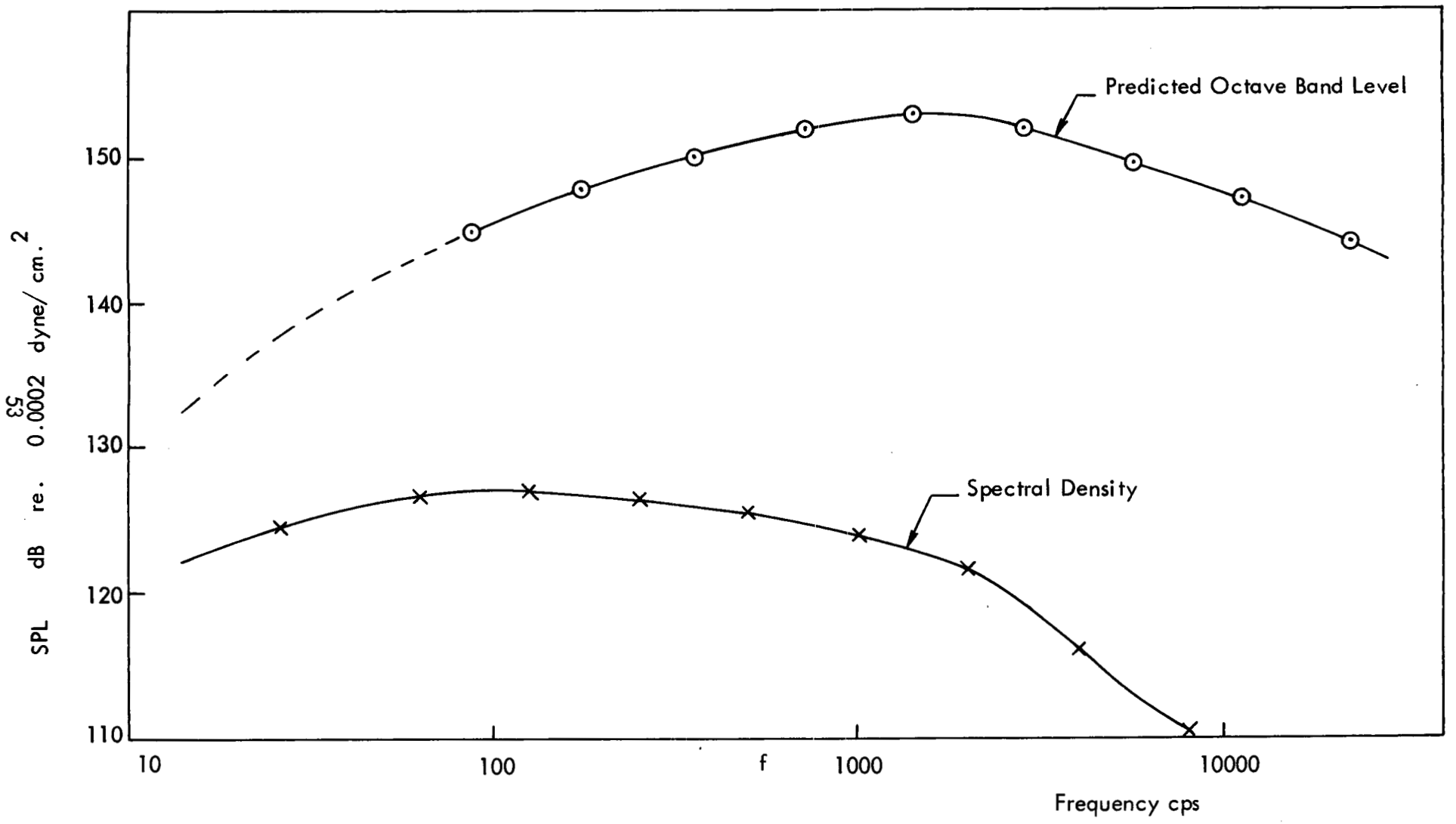

Figure 9. Predicted Frequency Spectrum for Pressure Fluctuations on SLA

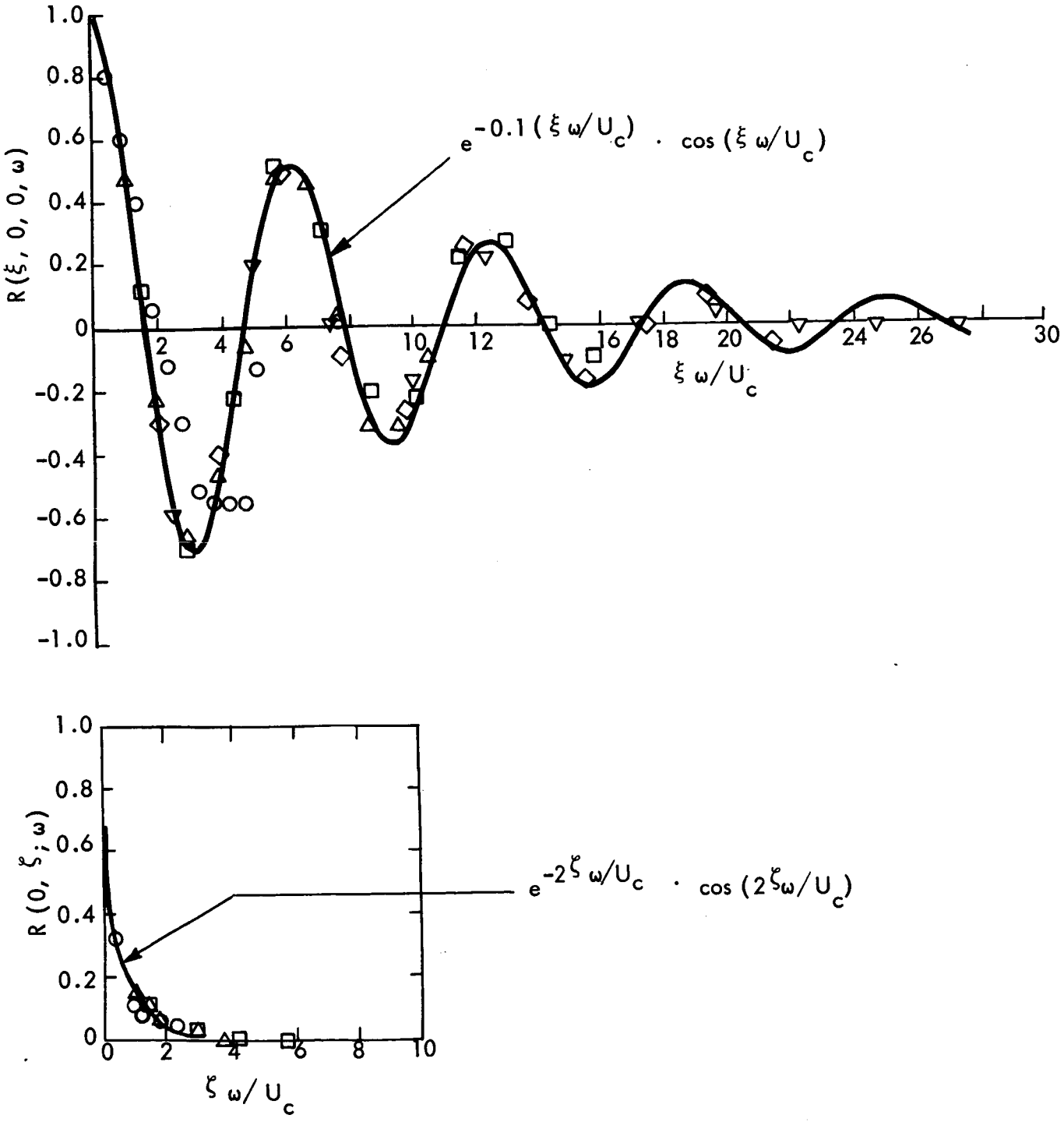

Figure 10. Narrow-Band Space Correlation of the Wall Pressure Fluctuations at M = 0.52. Center Frequency cps: ○, 1200; △, 2400; □, 3600; ◇, 4800; ▽, 6000

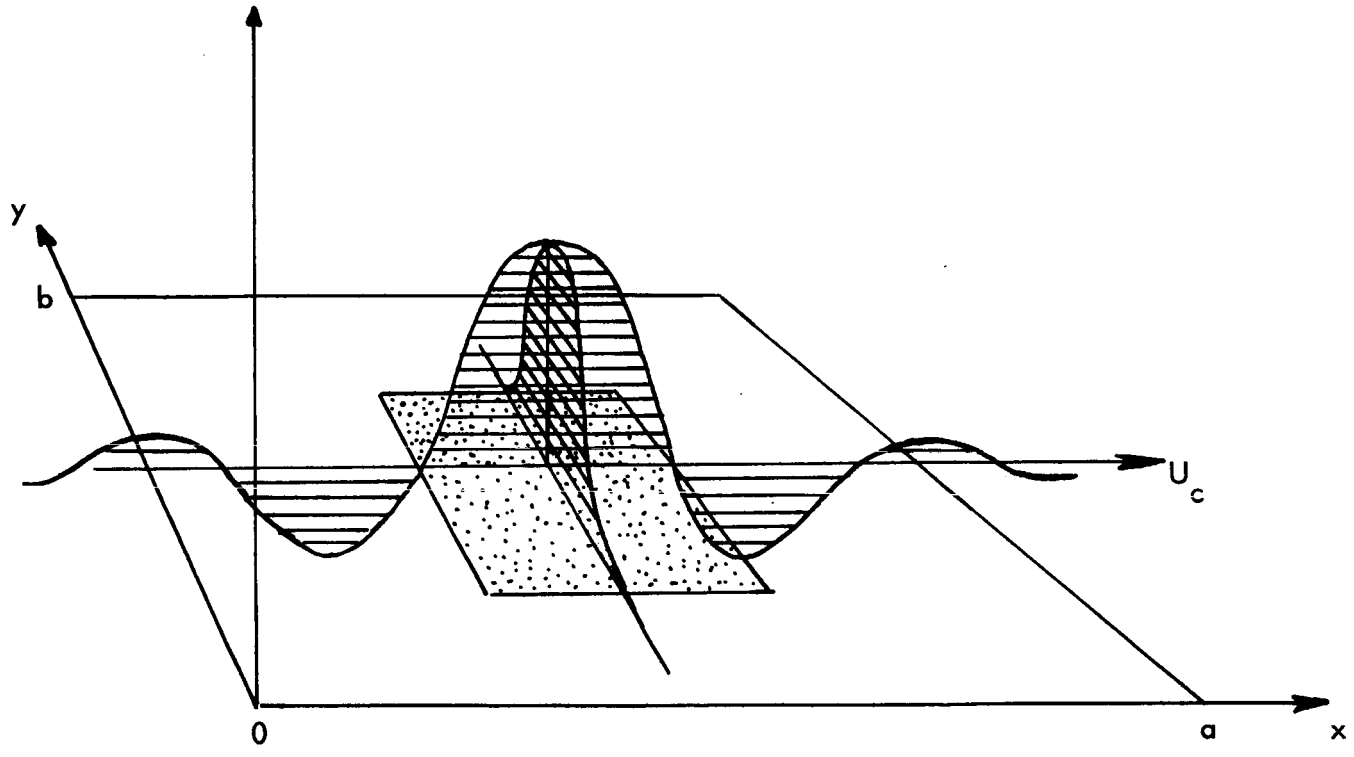

Figure 11. Geometry of Plate and Direction of Convected Turbulent Flow Showing Convected Correlation Pressure Pattern

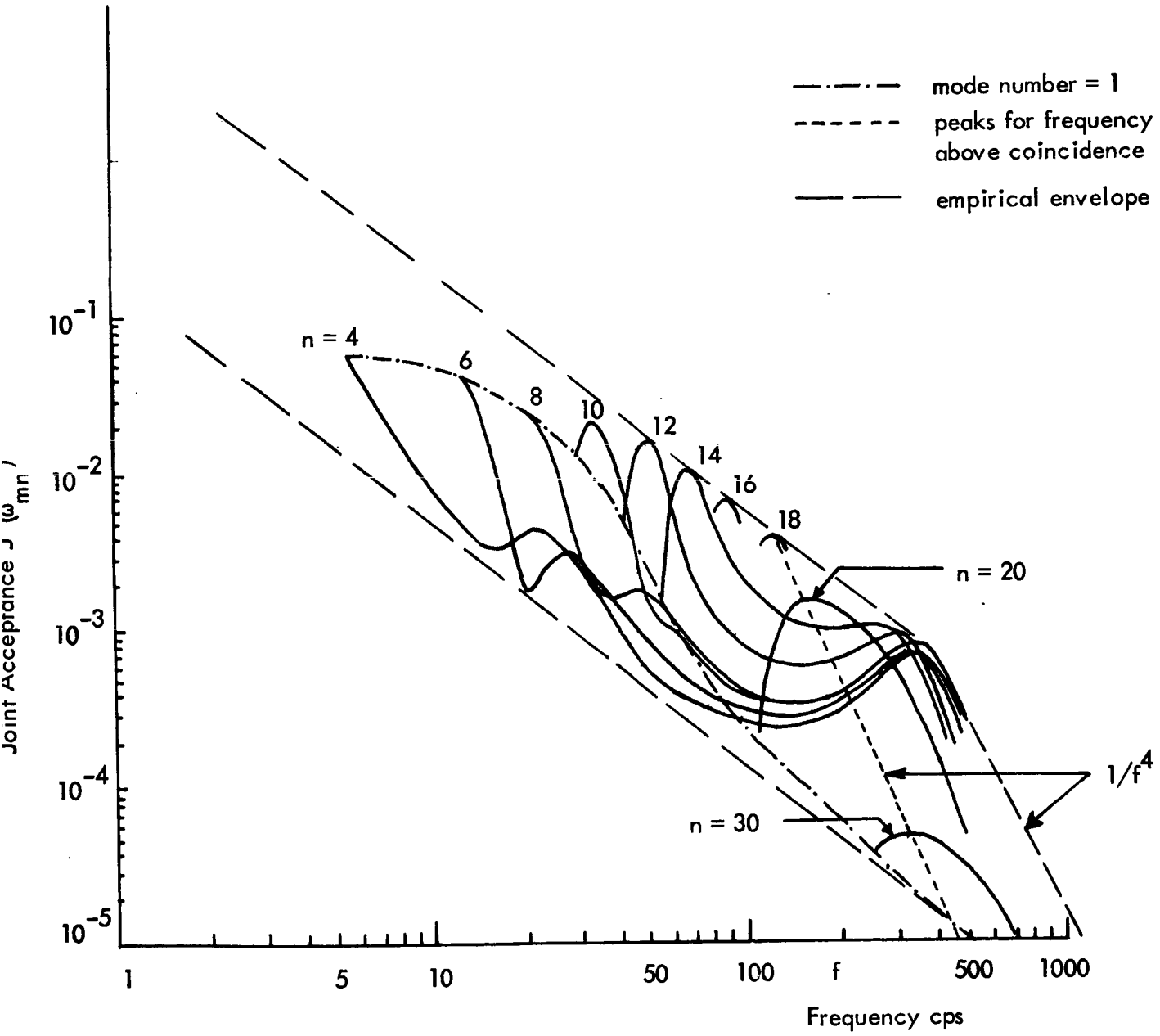

Figure 12. Variation of Joint Acceptance at Resonace with Frequency.

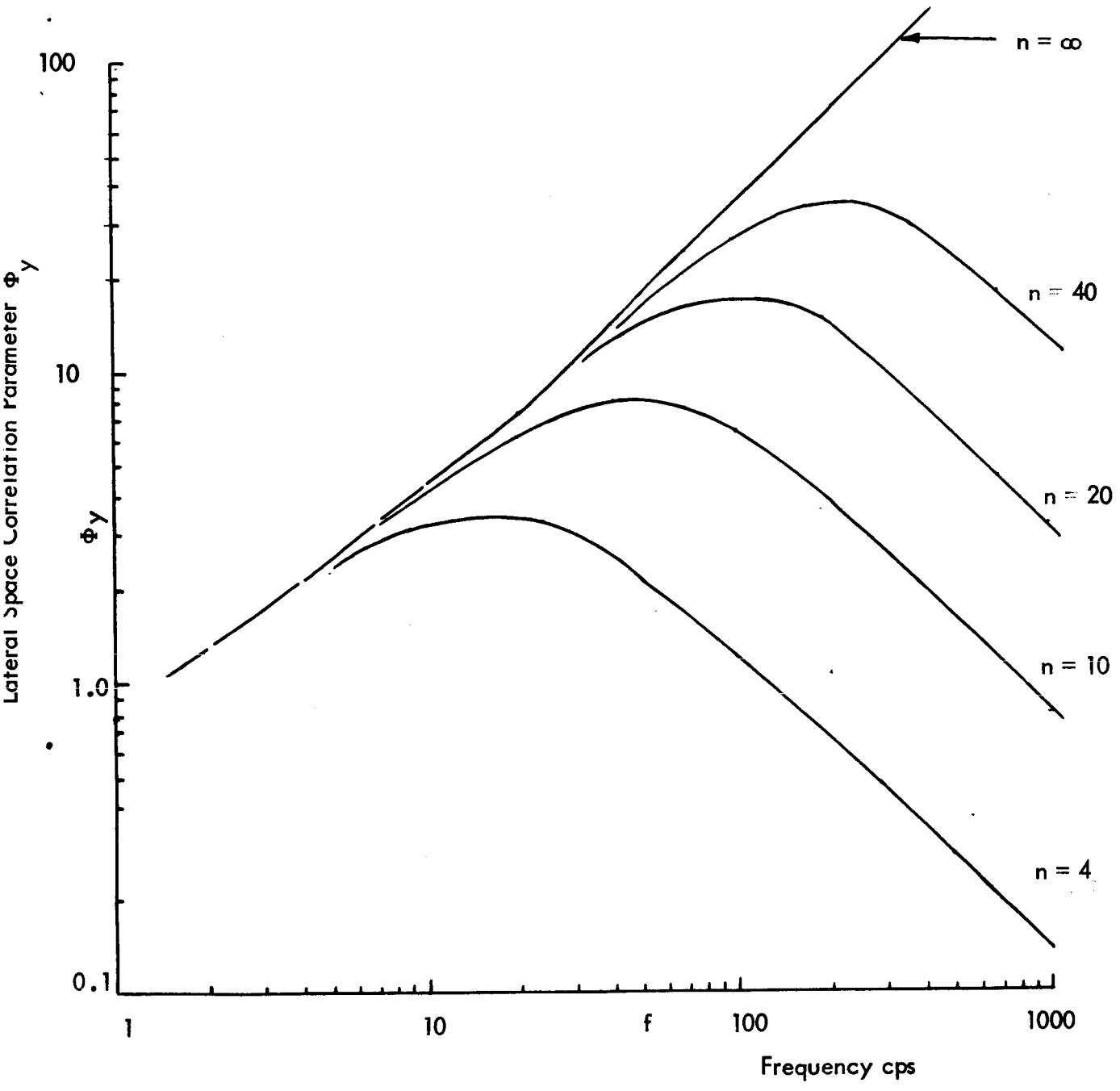

Figure 13. Variation of Parameter Φ_y with Frequency and Mode Number n.

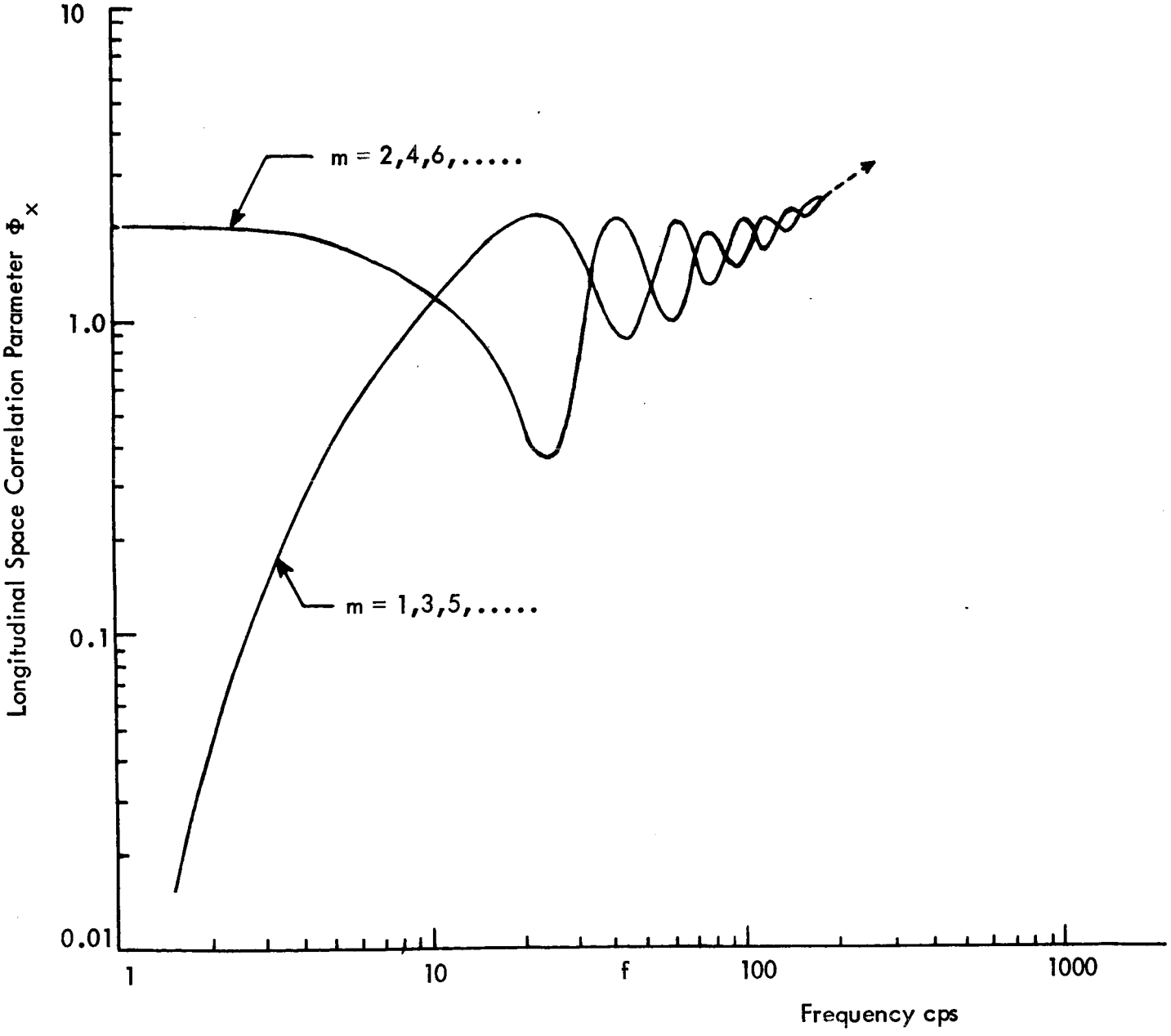

Figure 14. Variation of Parameter Φ_x with Frequency and Mode Number m.

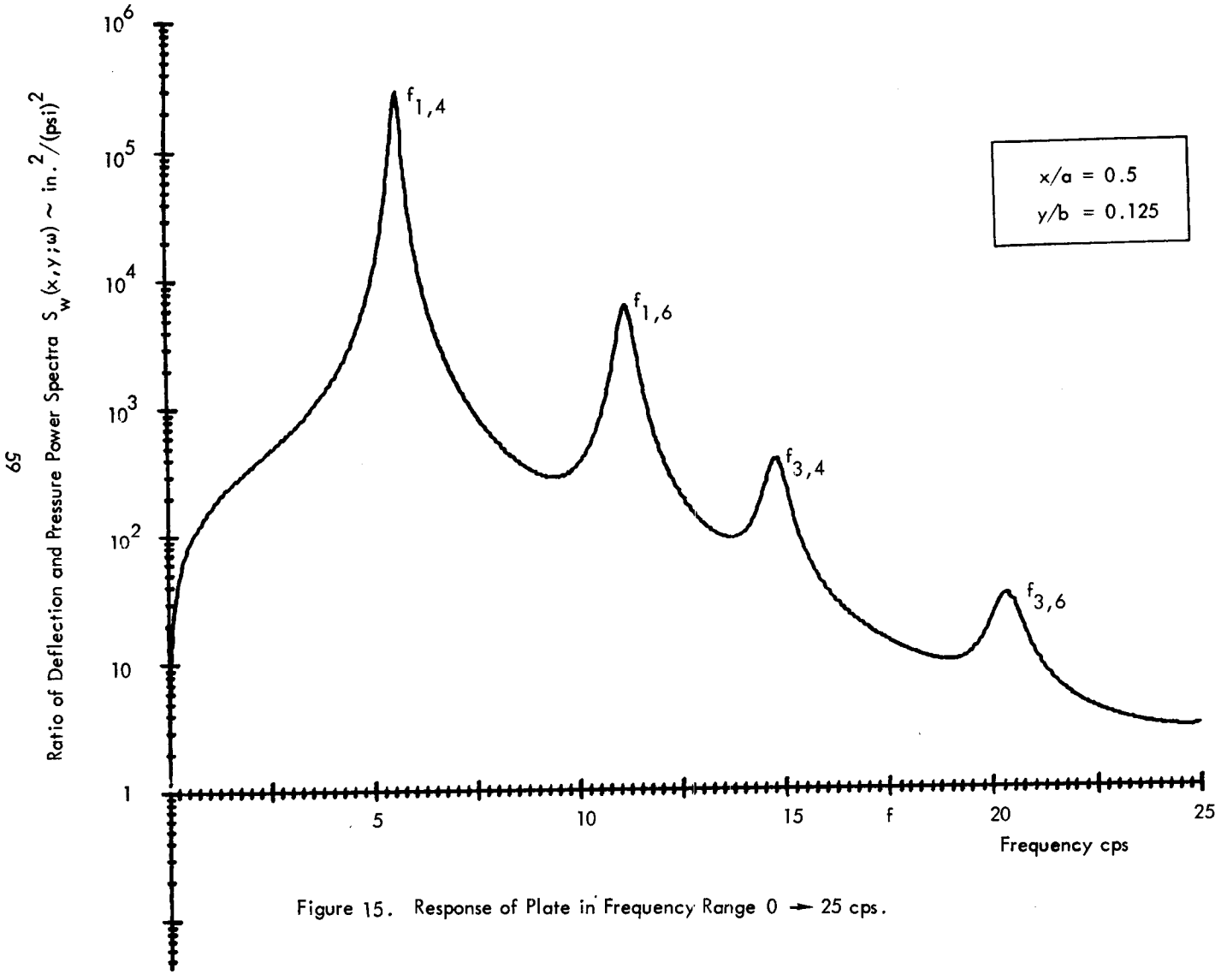

Figure 15. Response of Plate in Frequency Range 0 → 25 cps.

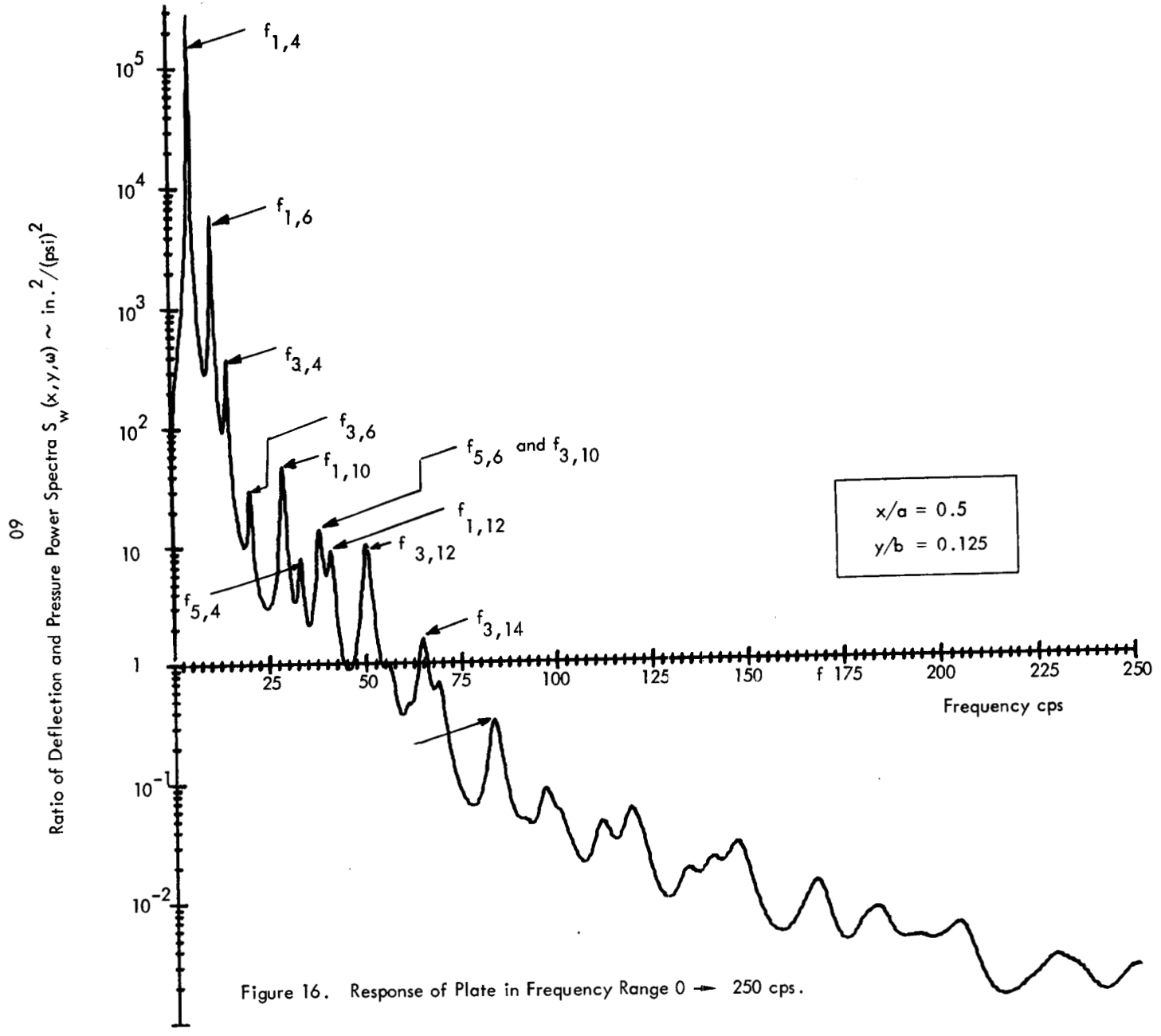

Figure 16. Response of Plate in Frequency Range 0 → 250 cps.

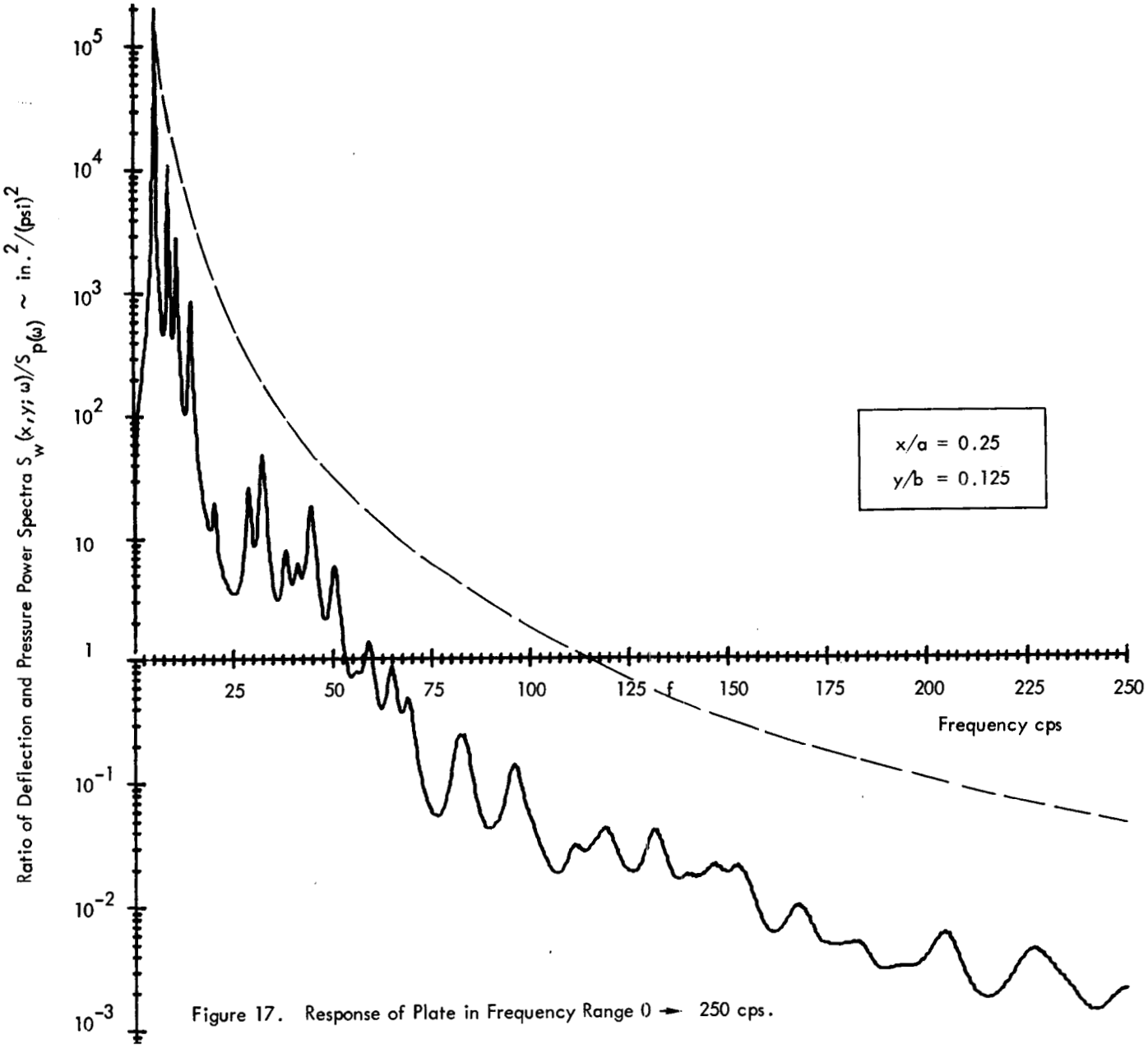

Figure 17. Response of Plate in Frequency Range 0 → 250 cps.

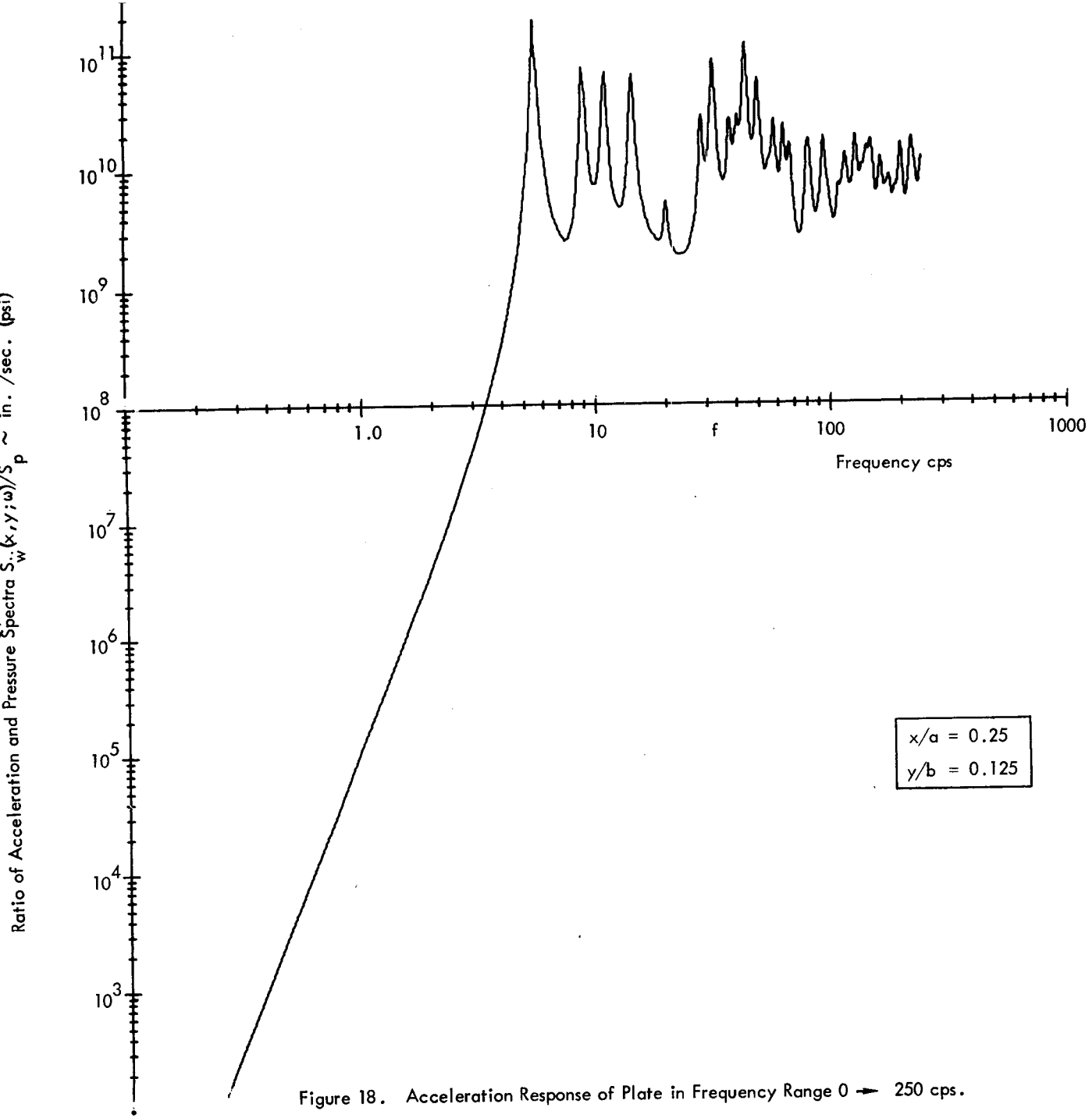

Figure 18. Acceleration Response of Plate in Frequency Range 0 → 250 cps.

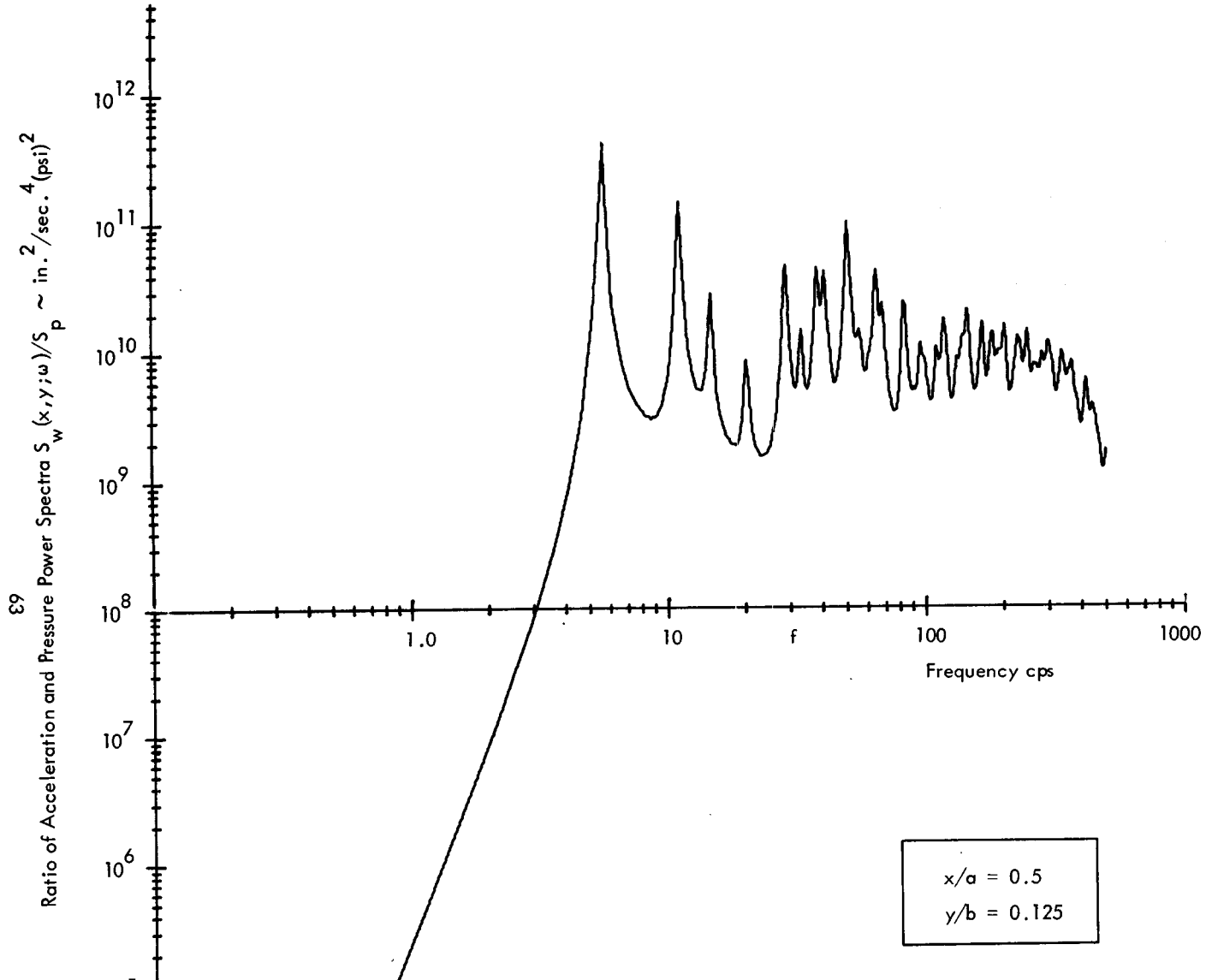

Figure 19. Acceleration Response of Plate in Frequency Range 0 → 500 cps.

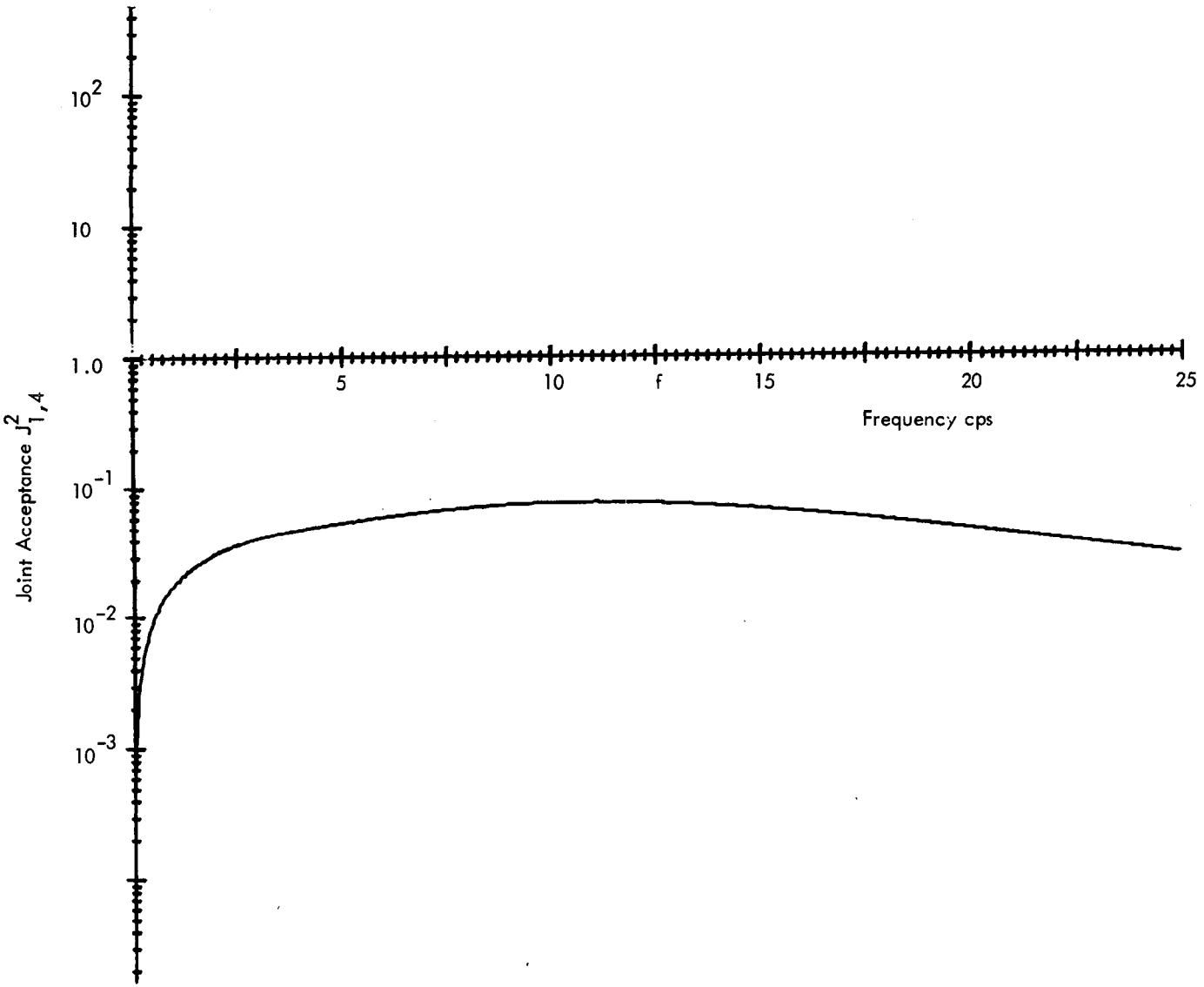

Figure 20. Joint Acceptance for First Mode ($f_{1,4}$).

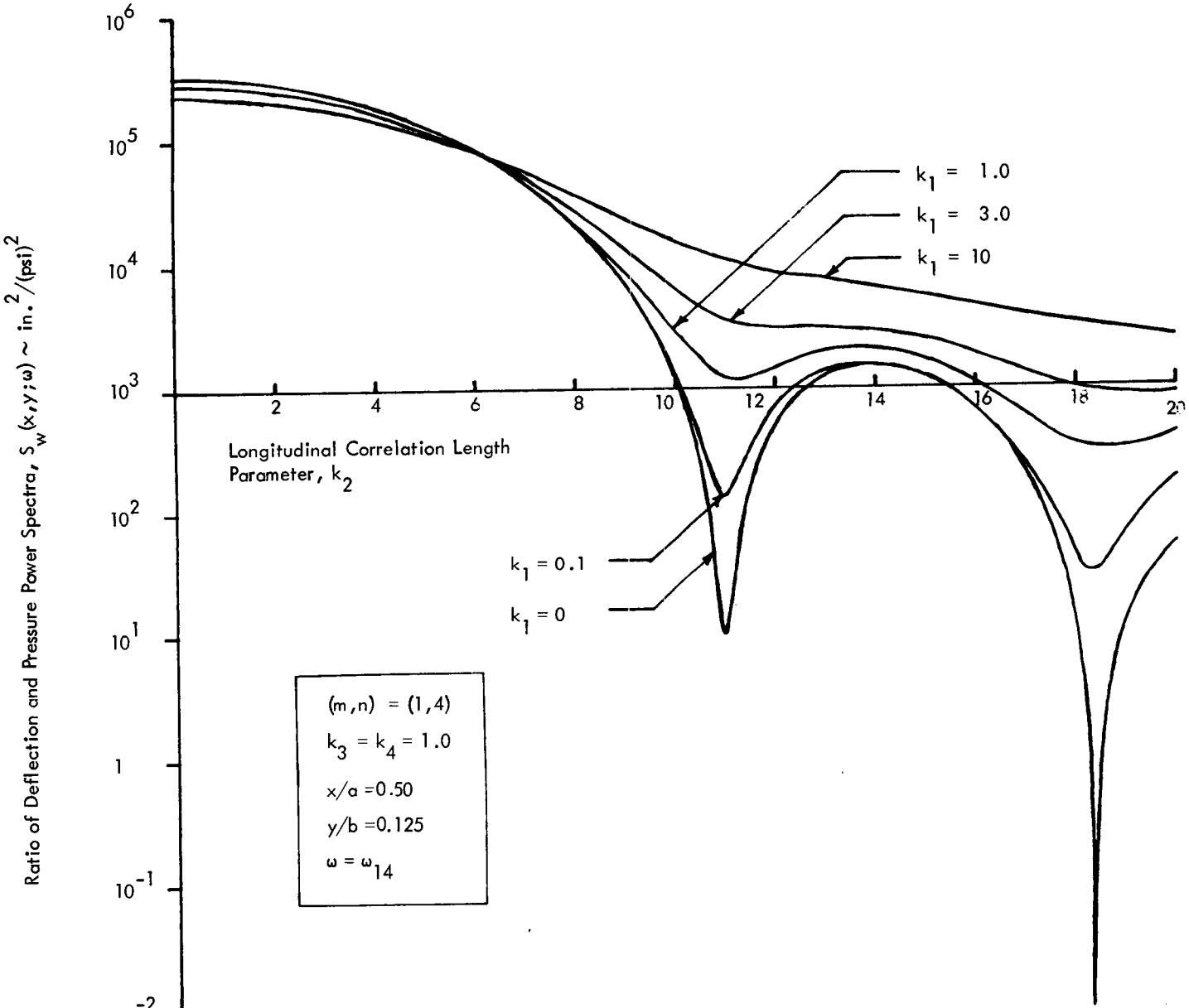

Fig. 21. Variation of Plate Response with Longitudinal Exponential Decay Parameter k_1 and Correlation Length Parameter k_2.

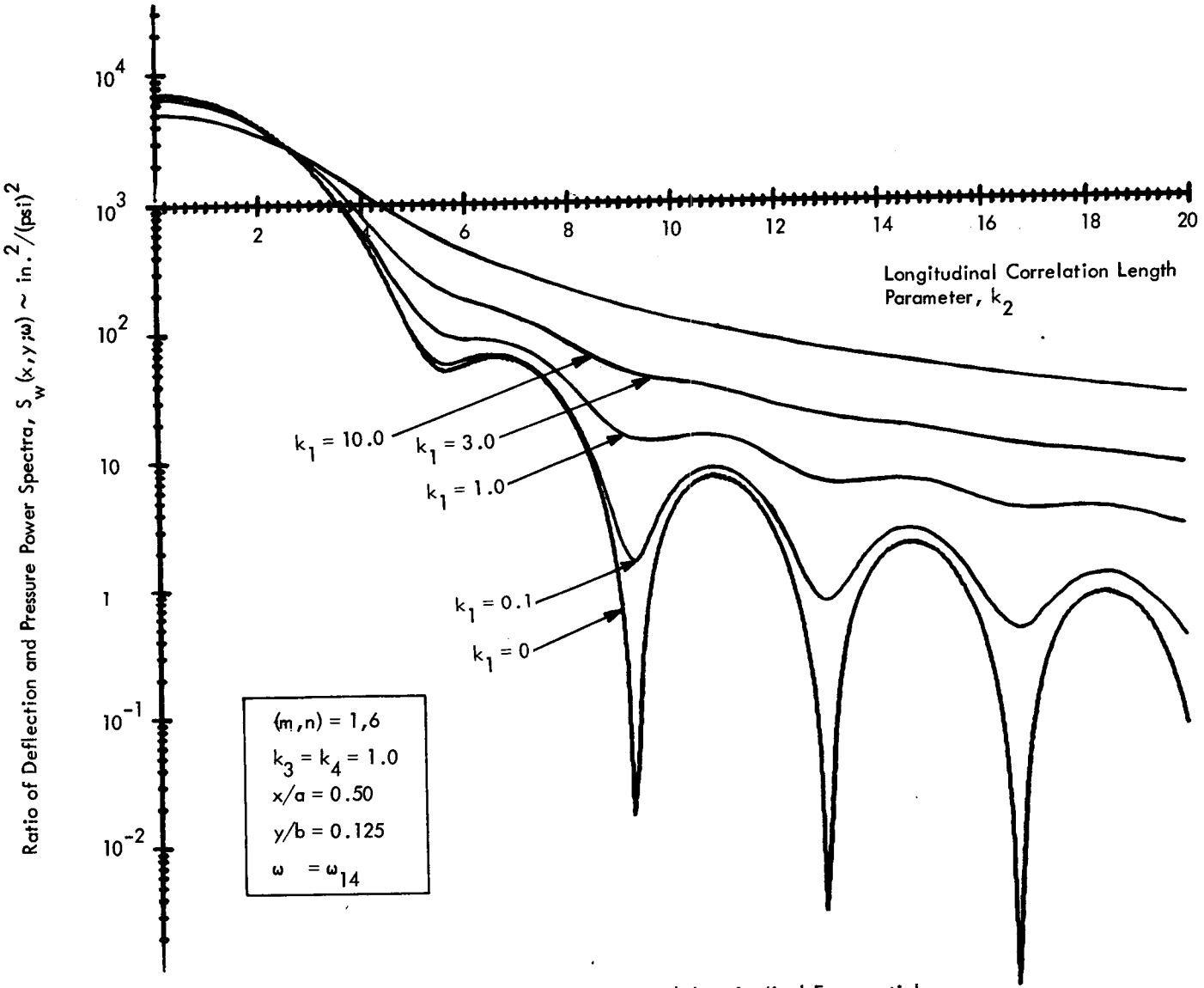

Figure 22. Variation of Plate Response with Longitudinal Exponential Decay Parameter k_1 and Correlation Length Parameter k_2.

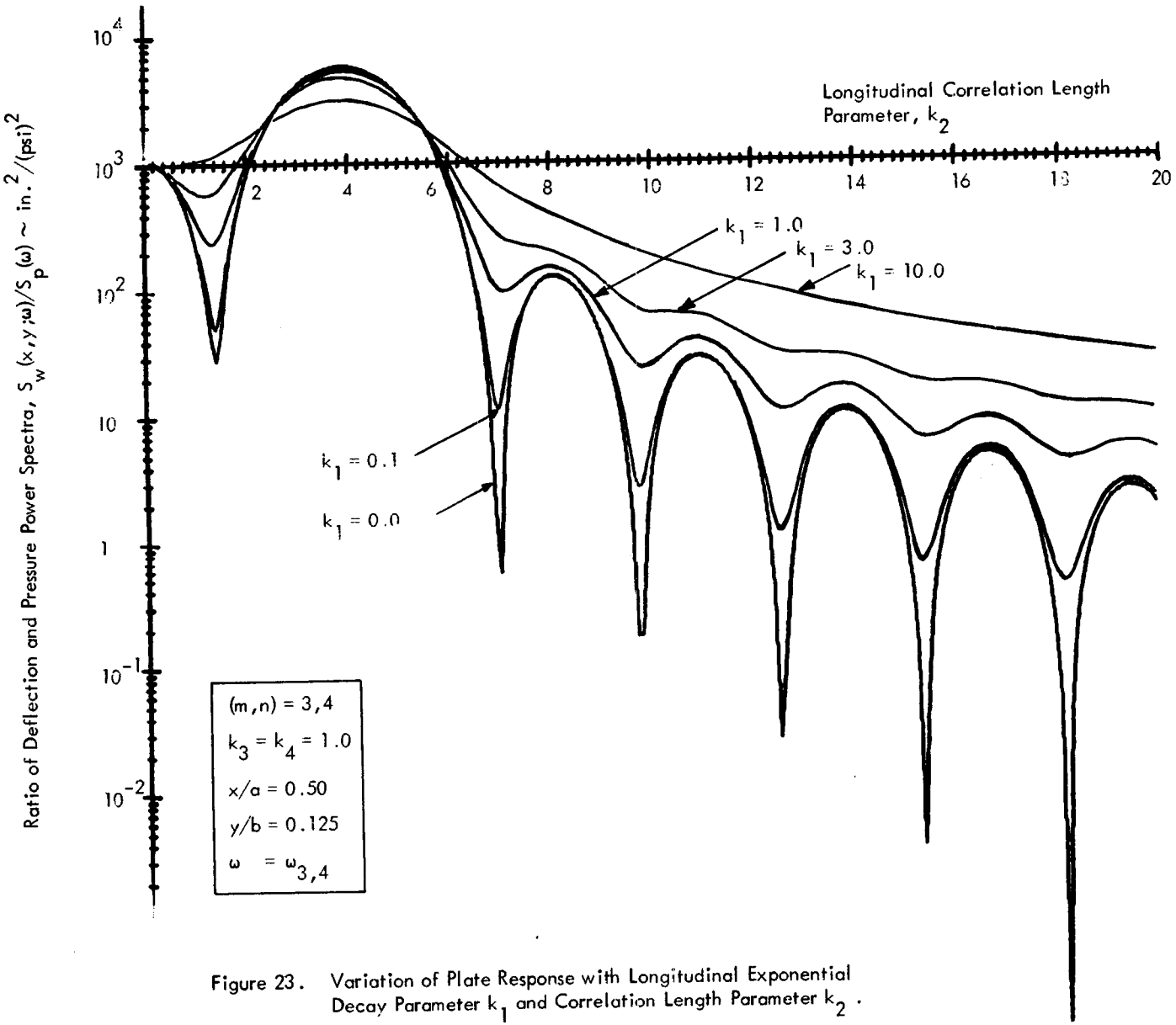

Figure 23. Variation of Plate Response with Longitudinal Exponential Decay Parameter k_1 and Correlation Length Parameter k_2.

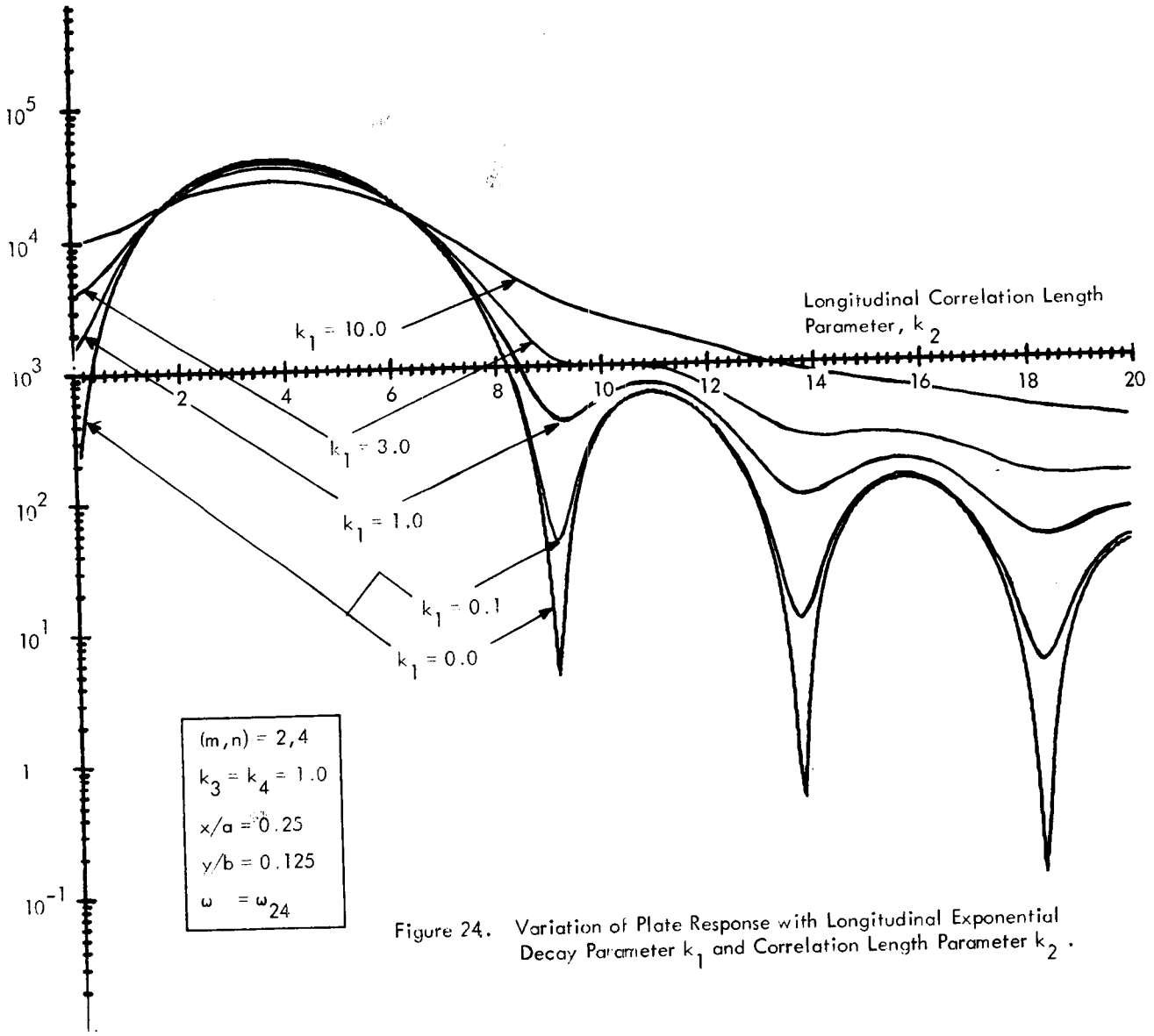

Figure 24. Variation of Plate Response with Longitudinal Exponential Decay Parameter k_1 and Correlation Length Parameter k_2.

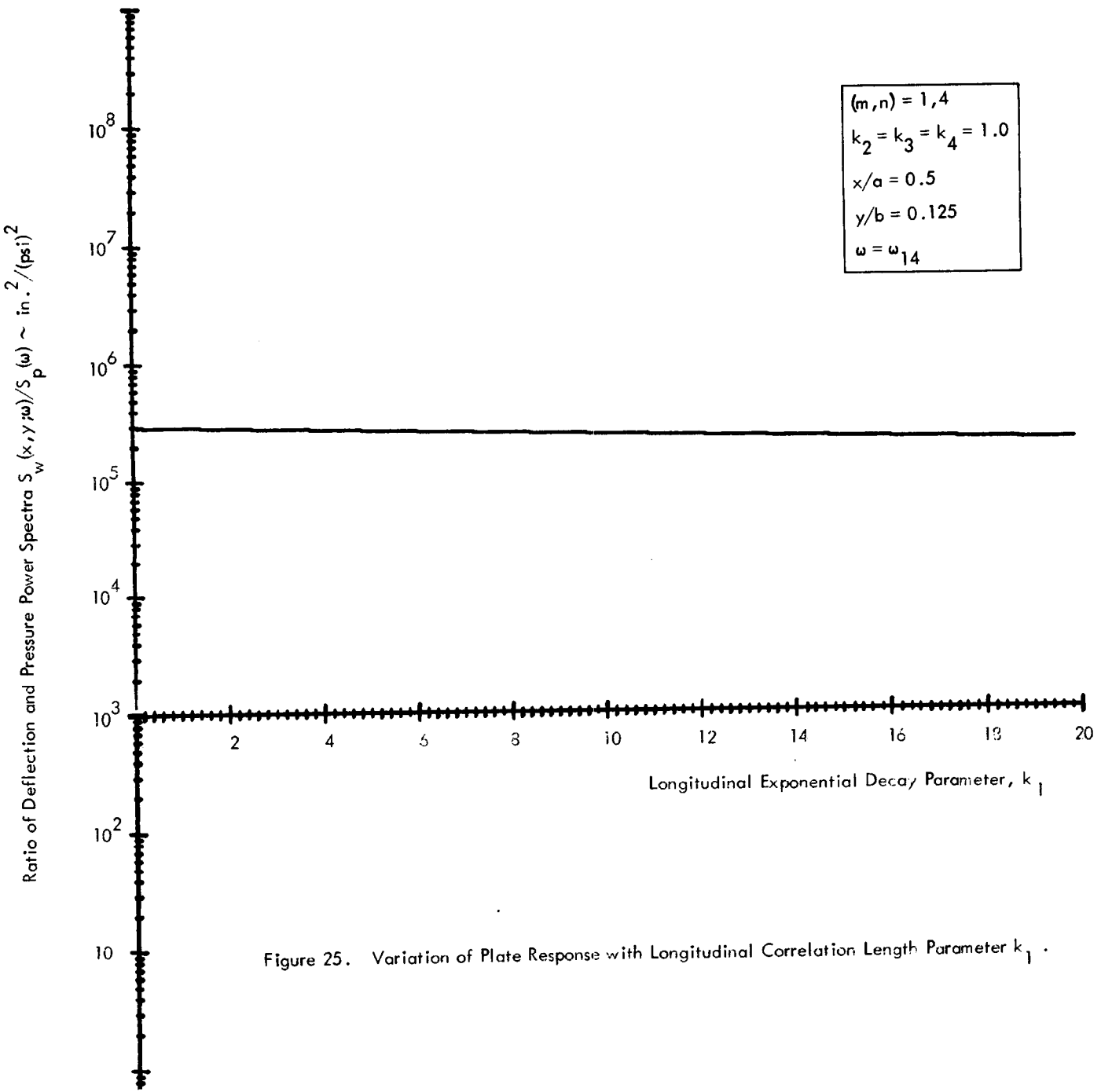

Figure 25. Variation of Plate Response with Longitudinal Correlation Length Parameter k_1.

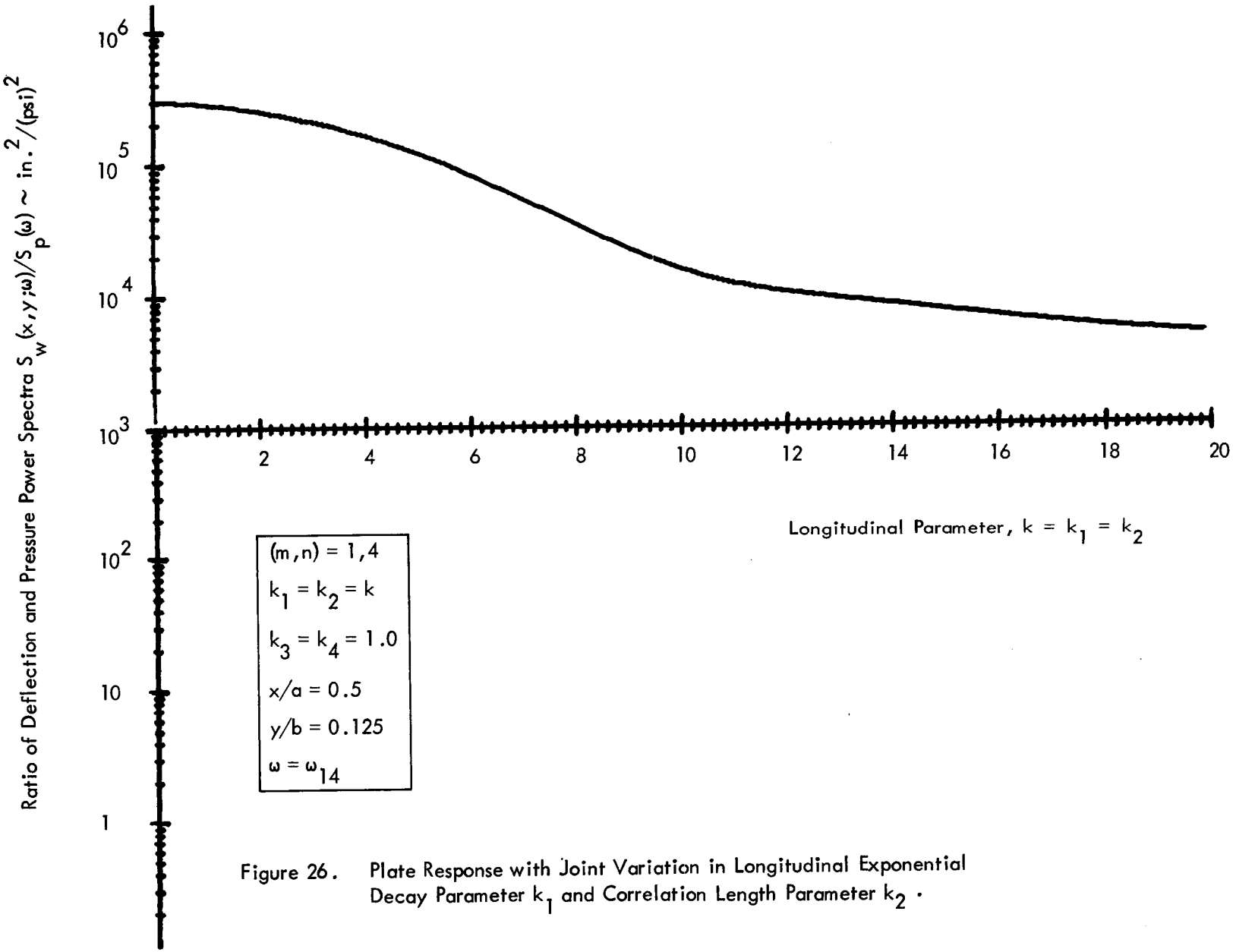

Figure 26. Plate Response with Joint Variation in Longitudinal Exponential Decay Parameter k_1 and Correlation Length Parameter k_2.

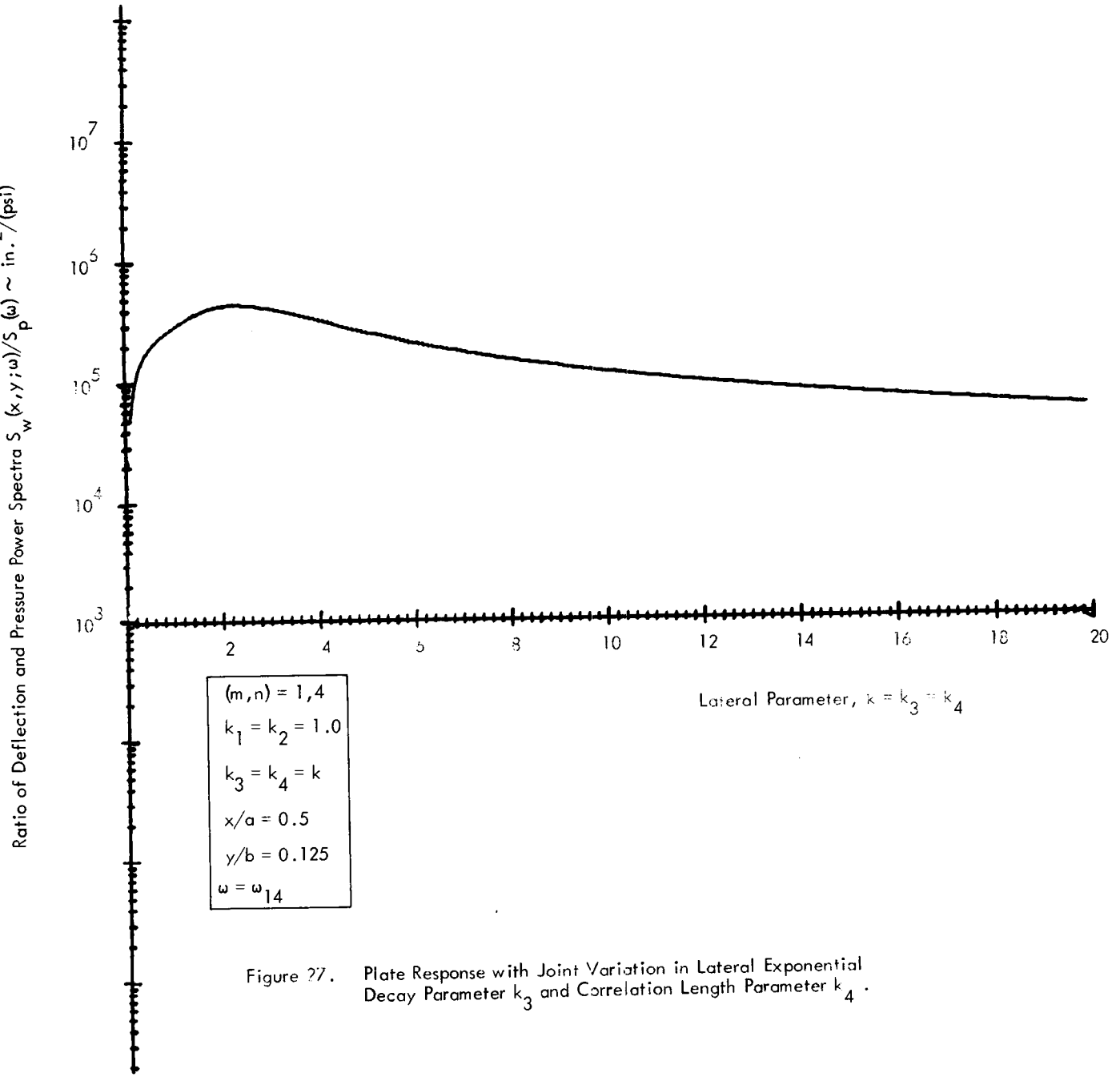

Figure 27. Plate Response with Joint Variation in Lateral Exponential Decay Parameter k_3 and Correlation Length Parameter k_4.

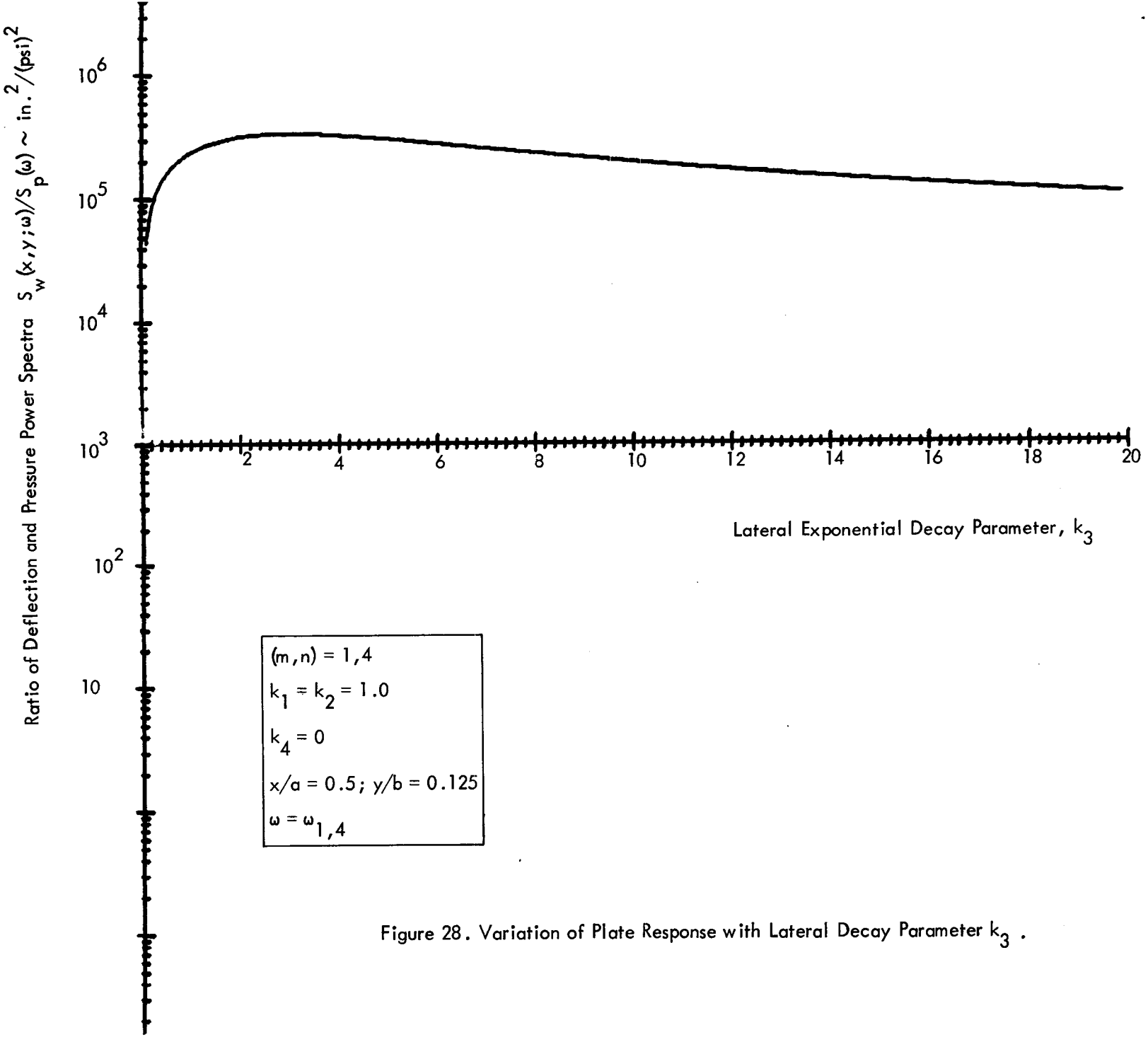

Figure 28. Variation of Plate Response with Lateral Decay Parameter k_3 .

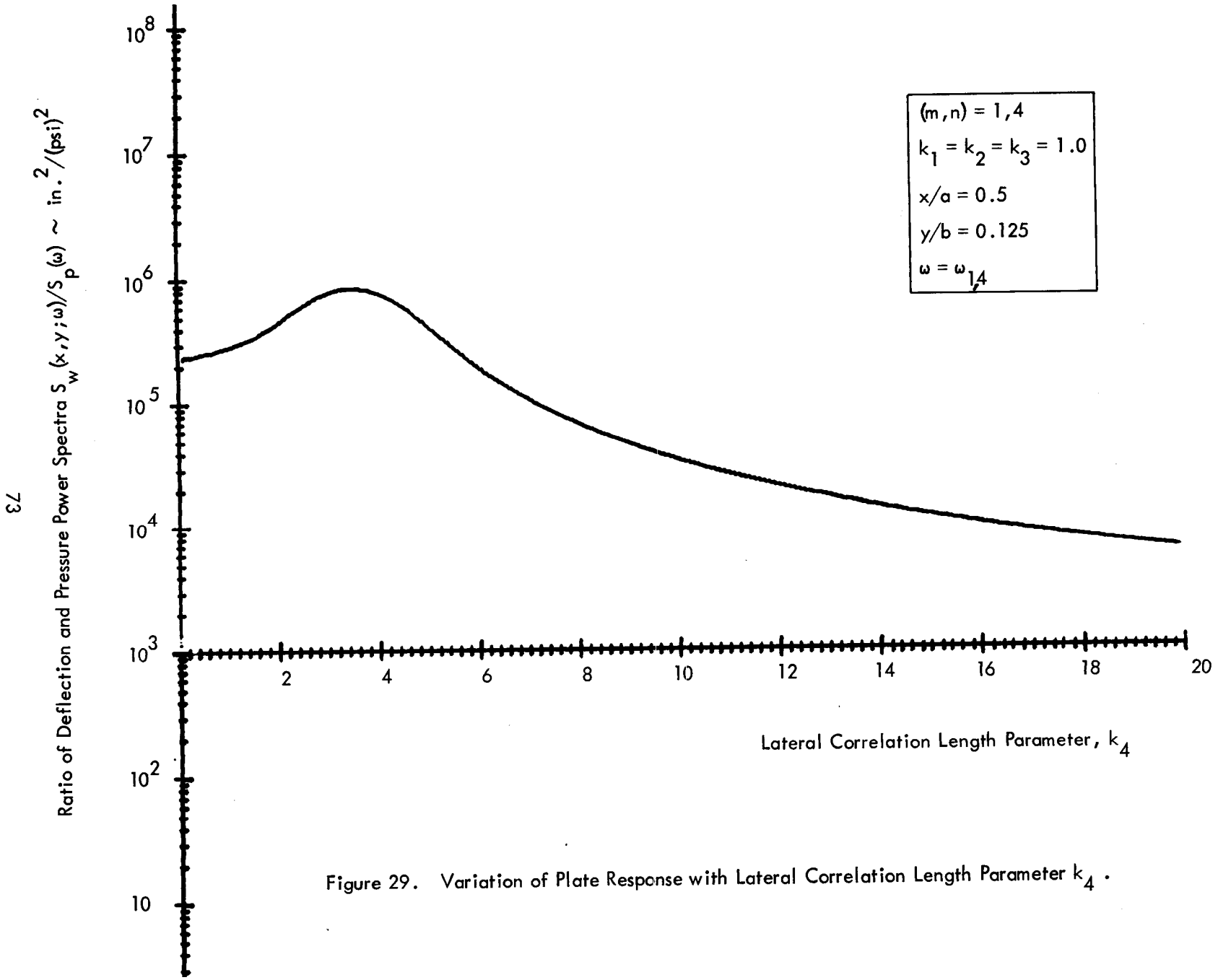

Figure 29. Variation of Plate Response with Lateral Correlation Length Parameter k_4.